Atmos. Chem. Phys., 24, 4473–4485, 2024
https://doi.org/10.5194/acp-24-4473-2024

Atmospheric Chemistry and Physics
Open Access
EGU

Formation and loss of light absorbance by phenolic aqueous SOA by ·OH and an organic triplet excited state

Stephanie Arciva[1], Lan Ma[1,a], Camille Mavis[1,b], Chrystal Guzman[1,c], and Cort Anastasio[1]

[1]Department of Land, Air and Water Resources, University of California, Davis, One Shields Avenue, Davis, CA 95616-8627, USA
[a]now at: SGS-CSTC Standards Technical Services Co. Ltd., Hangzhou, Zhejiang Province, 310052, China
[b]now at: Department of Atmospheric Science, Colorado State University, Fort Collins, CO 80521, USA
[c]now at: Department of Pharmacology, University of Washington, Seattle, WA 98195, USA

Correspondence: Cort Anastasio (canastasio@ucdavis.edu)

Received: 16 November 2023 – Discussion started: 21 November 2023
Revised: 28 February 2024 – Accepted: 2 March 2024 – Published: 17 April 2024

Abstract. Brown carbon (BrC) is an important component of biomass-burning (BB) emissions that impacts Earth's radiation budget. BB directly emits primary BrC as well as gaseous phenolic compounds (ArOH), which react in the gas and aqueous phases with oxidants – such as hydroxyl radical (•OH) and organic triplet excited states ($^3C^*$) – to form light-absorbing secondary organic aerosol (SOA). These reactions in atmospheric aqueous phases, such as cloud/fog drops and aerosol liquid water (ALW), form aqueous SOA (aqSOA), i.e., low-volatility, high-molecular-weight products. While these are important routes of aqSOA formation, the light absorption and lifetimes of the BrC formed are poorly characterized. To study these aspects, we monitored the formation and loss of light absorption by aqSOA produced by reactions of six highly substituted phenols with •OH and $^3C^*$. While the parent phenols absorb very little tropospheric sunlight, they are oxidized to aqSOA that can absorb significant amounts of sunlight. The extent of light absorption by the aqSOA depends on both the ArOH precursor and oxidant: more light-absorbing aqSOA is formed from more highly substituted phenols and from triplet reactions rather than •OH. Under laboratory conditions, extended reaction times in •OH experiments diminish sunlight absorption by aqSOA on timescales of hours, while extended reaction times in $^3C^*$ experiments reduce light absorption much more slowly. Estimated lifetimes of light-absorbing phenolic aqSOA range from 3 to 17 h in cloud/fog drops, where •OH is the major sink, and from 0.7 to 8 h in ALW, where triplet excited states are the major sink.

1 Introduction

Organic aerosols (OAs) account for 20 % to 90 % of airborne particulate mass (Jimenez et al., 2009; Kanakidou et al., 2005), with significant effects on climate (Heald et al., 2008; Shrivastava et al., 2017) and human health (Aguilera et al., 2021; Kim et al., 2015; Zhou et al., 2021). Types of OAs include primary OA (POA), which is directly emitted from sources such as biomass burning and fossil fuel combustion (Andreae, 2019; Bond et al., 2004), and secondary OA (SOA), which is formed from atmospheric aging in the gas or condensed phases (Graber and Rudich, 2006; Jimenez et al., 2009; Powelson et al., 2014; Volkamer et al., 2006). SOA usually accounts for a dominant fraction of the OA budget (Hallquist et al., 2009; Robinson et al., 2007). Biomass burning (BB) is a significant source of POA as well as reactive organic gases that form SOA (Akagi et al., 2011; Andreae, 2019; Bond et al., 2004; Hallquist et al., 2009), which together affect air quality, atmospheric composition, and climate (Garofalo et al., 2019; Kleinman et al., 2020; O'Dell et al., 2021).

While most OA scatters sunlight, brown carbon (BrC, i.e., light-absorbing organic carbon) absorbs sunlight and possibly causes warming (Jo et al., 2016; Reid et al., 2005; Zhang et al., 2020). Compared to black carbon, which strongly absorbs sunlight across the UV–Vis spectrum, light absorption by BrC is strongly wavelength dependent, increasing from the visible to the UV (Hecobian et al., 2010; Laskin et al., 2015). BB is an important source of BrC that strongly absorbs light (Di Lorenzo et al., 2017; Kirchstetter and Thatcher, 2012; Palm et al., 2020; Zhong and Jang, 2014). POA and SOA formed from smog chamber experiments of biomass burning emissions show evidence of light absorption by BrC, especially in the near-UV region (Saleh et al., 2013). The absorption of BrC is affected by atmospheric oxidation, exposure to sunlight, and pH, as well as brown carbon source (Grieshop et al., 2009; Hennigan et al., 2011; Liu et al., 2021; Ortega et al., 2013). Also, atmospheric aging can increase both light absorption by forming chromophores and photo-bleach chromophoric molecules (Fleming et al., 2020; Hems et al., 2020, 2021; Schnitzler et al., 2022; Zhao et al., 2015; Zhong and Jang, 2014).

One important class of reactive organic gases potentially important for secondary BrC formation is phenols, which we abbreviate as ArOH (Andreae, 2019; Chang and Thompson, 2010). ArOH are abundant emissions from BB, with high emissions of simple phenols and smaller amounts of highly substituted ArOH (Andreae, 2019; Schauer et al., 2001). ArOH typically have strong absorbance peaks under 300 nm that fall exponentially at longer wavelengths (Kaeswurm et al., 2021), although phenols with carbonyl or nitro substituents can absorb sunlight (Smith et al., 2016; Wang et al., 2022). Phenols rapidly undergo photochemical transformations both in the gas and aqueous phases with various oxidants to produce low-volatility compounds (Berndt and Böge, 2003; Gurol and Nekouinaini, 1984; Ma et al., 2021; Sun et al., 2010; Yee et al., 2013; Yu et al., 2014). ArOH from BB have a wide range of Henry's law constants (K_H). Highly substituted ArOH with modest to high K_H values (10^3–10^8 M atm^{-1}) will have a higher tendency to partition into the aqueous phase (McFall et al., 2020), where they can be oxidized to form large low-volatility products (Smith et al., 2016; Yu et al., 2016).

Atmospheric aqueous oxidants that rapidly oxidize ArOH during the daytime include hydroxyl radical ($^{\bullet}$OH) and organic triplet excited states (^{3}C*) (Smith et al., 2015). Both simple and highly substituted phenols react rapidly with $^{\bullet}$OH and ^{3}C*, with second-order rate constants of roughly 10^9 and 10^8 M^{-1} s^{-1} at pH 5, respectively (Arciva et al., 2022; Buxton et al., 1988; Ma et al., 2021; Smith et al., 2015). Additionally, both the $^{\bullet}$OH and ^{3}C* reactions efficiently form aqueous SOA (aqSOA), with average ($\pm 1\sigma$) mass yields of 82($\pm$12) % and 83($\pm$14) %, respectively (Arciva et al., 2022; Ma et al., 2021). SOA mass yields for ArOH oxidation in the aqueous phase are often higher than the parallel gas-phase reactions (Arciva et al., 2022; Berndt and Böge, 2003; Coeur-Tourneur et al., 2010; Ma et al., 2021), a result of more efficient oligomerization and functionalization reactions in the aqueous phase (Yu et al., 2016) as opposed to the more common fragmentation in the gas phase. Additionally, aqueous reactions produce oligomers, i.e., low-volatility, conjugated products that can significantly enhance light absorption (Chang and Thompson, 2010; Huang et al., 2018; Li et al., 2014; Yu et al., 2016).

While the processing of ArOH is a significant source of light-absorbing aqSOA, little is known about how phenol-derived brown carbon is photobleached with continued reaction. In part, this likely depends on which oxidant produced the aqSOA, as reaction products can be quite different. Initial oxidation of ArOH by $^{\bullet}$OH and ^{3}C* forms aqSOA that absorbs light above 300 nm (Jiang et al., 2023b; Li et al., 2022). ArOH reactions with $^{\bullet}$OH initially produce abundant hydroxylated analogues, while ^{3}C* oxidation of ArOH dominantly forms oligomers (Misovich et al., 2021; Yu et al., 2016). However, the extended aging processes for phenolic brown carbon may vary since chromophores of different chemical composition react differently to photooxidation (Li et al., 2022). In cloud and fog conditions, extended $^{\bullet}$OH reactions transform phenolic aqSOA chromophores more rapidly compared to reactions with ^{3}C* (Jiang et al., 2023b). However, in more concentrated conditions of particle water, the concentrations of $^{\bullet}$OH and ^{3}C* are different than under the dilute conditions of cloud and fog drops (Ma et al., 2023, 2024), which likely affects the lifetimes of phenolic brown carbon.

In this study, we monitored the formation and loss of light absorption by aqueous SOA formed by reactions of six highly substituted BB phenols with $^{\bullet}$OH and ^{3}C*. We determined mass absorption coefficients (MACs) for the parent ArOH and for the evolving aqSOA as a function of reaction time. We also calculated the rate of sunlight absorption by aqSOA throughout the course of each reaction and the lifetimes of this absorbance in our experiments as well as for estimated cloud and particle water conditions.

2 Experiment

2.1 Chemicals

Chemicals were used as received. Hydrogen peroxide (H_2O_2, 30 % solution in water), 3,4-dimethoxybenzaldehyde (DMB, 99 %), 4-hydroxy-3-methoxyphenylacetone (guaiacyl acetone, GA, 96 %), 4-(hydroxymethyl)-2-methoxyphenol (vanillyl alcohol, VAL, $\geq$ 98 %), 2-(4-hydroxyphenyl)ethanol (tyrosol, TYR, 98 %), 4-hydroxy-3,5-dimethoxybenzoic acid (syringic acid, SyrAcid, $\geq$ 95 %), 3-(4-hydroxy-3-methoxyphenyl)prop-2-enoic acid (*trans*-ferulic acid, FA, 99 %), and 2-nitrobenzaldehyde (2NB, 98 %) were purchased from Sigma-Aldrich. Upon illumination, *trans*-FA photoisomerizes to a 41 : 58 mixture of the *cis*- and *trans*-isomers; our experiments were performed

on this mixture. (3,5-dimethoxy-4-hydroxyphenyl)acetone (syringyl acetone, SA, 82 %) was synthesized by Carbosynth LLC. Sulfuric acid (trace metal grade) and acetonitrile (Optima LC-MS grade) were from Fisher Scientific. Chemical solutions were prepared in air-saturated ultrapure Milli-Q water ($\geq 18.2\,\mathrm{M\Omega\,cm}$) from a Millipore Advantage A10 system with an upstream Barnstead activated carbon filter.

2.2 Reaction solutions

Fresh air-saturated solutions were prepared daily containing 50 or 100 µM ArOH and either 5 or 10 mM H_2O_2 (as an $^{\bullet}$OH precursor) or 5 or 10 µM DMB (as a ^{3}C* precursor) (Table S1 in the Supplement). Solutions were adjusted to pH 5 using sulfuric acid, and ∼ 20 mL was transferred to an airtight 5 cm quartz cuvette. Solutions were illuminated at 20 °C with constant stirring in a solar simulator equipped with a 1000 W Xenon lamp with three downstream optical filters: a water filter, an AM1.0 air mass filter (AM1D-3L, Sciencetech), and a 295 nm long-pass filter (20CGA-295, Thorlabs); see Fig. S1 in the Supplement for a typical photon flux.

During illumination we periodically removed aliquots of sample and measured the ArOH concentration using high-performance liquid chromatography (HPLC: Shimadzu LC-20AB pump, Thermo Scientific Accucore XL C_{18} column (50×3 mm, 4 µm bead), and Shimadzu SPD-M20A photodiode array detector). HPLC conditions (eluent, flow rate, detection wavelengths) are described elsewhere (Arciva et al., 2022). We sampled to approximately three phenol half-lives, i.e., to $\sim 3t_{1/2}$, when roughly 12 % of the initial phenol remained. We report times for each aliquot removal in Table S1 and show phenol decay kinetics in Fig. S2. We measured dark controls in a separate temperature-controlled dark chamber at 20 °C with constant stirring; there was no phenol loss in the dark. Additionally, three phenols (SA, SyrAcid, and FA) undergo direct photodegradation, which contributed to 6 % to 35 % of measured ArOH loss (Fig. S3).

At each time point we also measured light absorption by removing the sample cell from the illumination system and taking a UV–Vis spectrum in a Shimadzu UV-2501PC spectrophotometer baselined with Milli-Q water adjusted to pH 5 with sulfuric acid. Absorbance measurements were baseline corrected and represent the absorbance of reaction mixtures (i.e., parent ArOH, oxidant precursor, and aqSOA formed). Molar absorption coefficients for the six phenols are in Table S2 and shown graphically in Fig. S4. Absorbance of the mixtures during reaction is shown in Fig. S5 for the $^{\bullet}$OH reactions and Fig. S6 for the ^{3}C* reactions.

2.3 Oxidant concentrations

Using measured ArOH decay kinetics, we estimated the steady-state concentration of oxidant in each experiment. We first determined the pseudo-first-order decay rate constant (k'_{light}) for phenol loss by $^{\bullet}$OH or ^{3}C* as the negative value of the slope of a plot $\ln(\frac{[\mathrm{ArOH}]t}{[\mathrm{ArOH}]_o})$ versus reaction time, where $[\mathrm{ArOH}]_t$ and $[\mathrm{ArOH}]_0$ are the phenol concentrations at times t and zero (Fig. S2). Next, we normalized k'_{light} to sunlight conditions at midday on the winter solstice at Davis and corrected for any direct photodegradation using

$$k'_{\mathrm{ArOH}} = \left[\left(\frac{k'_{\mathrm{light}}}{j_{\mathrm{2NB,exp}}}\right) \times j_{\mathrm{2NB,win}}\right] - j_{\mathrm{ArOH}}. \quad (1)$$

In this equation, k'_{ArOH} is the normalized rate constant for phenol loss, j_{2NB} is the first-order decay rate constant for loss of 2NB (our actinometer) on the day of the phenol experiment, $j_{\mathrm{2NB,win}}$ is the value measured at midday on the winter solstice in Davis, $0.0070\,\mathrm{s}^{-1}$ (Anastasio and McGregor, 2001), and j_{ArOH} is the rate constant for direct photodegradation of ArOH. Rate constants are summarized in Table S3 and S4. We then estimated the concentration of oxidant in each solution by dividing k'_{ArOH} by the second-order rate constant for phenol reacting with $^{\bullet}$OH or ^{3}C*, which are from our previous works (Arciva et al., 2022; Ma et al., 2021). Since triplet solutions can also form $^{\bullet}$OH and singlet molecular oxygen ($^1O_2$*), we estimated the potential contributions of these secondary oxidants to phenol loss. As described in Sect. S1 of the Supplement, these oxidants appear to be negligible sinks for ArOH in our triplet experiments.

2.4 Mass absorption coefficients, rate of sunlight absorption by aqSOA, and lifetime of aqSOA light absorbance

Mass absorption coefficients (MACs; $\mathrm{m^2\,g^{-1}}$) for the aqSOA at each sampling time were determined at each wavelength λ using

$$\mathrm{MAC}_{\mathrm{aqSOA},\lambda}\left(\mathrm{m^2\,g^{-1}}\right) = \frac{2.303 \times \mathrm{Abs}_{\mathrm{aqSOA},\lambda} \times 10^3 \times 10^{-4}}{l \times (Y_{\mathrm{SOA}} x\, \Delta[\mathrm{ArOH}])}, \quad (2)$$

where 2.303 converts the absorbance from base-10 to base-e; $Abs_{\mathrm{aqSOA},\lambda}$ is the absorbance of the solution at wavelength λ, corrected to remove the absorbances from the oxidant precursor and remaining parent phenol (see Sect. S2); l is the path length of our cuvette (5 cm); Y_{SOA} is the aqSOA mass yield during oxidation of ArOH with $^{\bullet}$OH or ^{3}C* (Arciva et al., 2022; Ma et al., 2021), which were determined using high-resolution aerosol mass spectrometry (AMS) and are summarized in Table S5; and Δ[ArOH] is the decrease in phenol mass concentration (in $\mathrm{g\,L^{-1}}$) between times zero and t. The factor of 10^3 is converted from L to $\mathrm{cm^3}$, while the factor of 10^{-4} is converted from $\mathrm{cm^2}$ to $\mathrm{m^2}$. The MAC values for each of the six highly substituted parent phenols were calculated as described in Sect. S2 of the Supplement.

We calculated the overall rate of sunlight absorption by aqSOA (R_{abs}) at a given time point by multiplying the cor-

responding MAC_{aqSOA} by the modeled actinic flux and summing from 280 to 800 nm:

$$R_{abs}\left(\text{mol photon g}^{-1}\,\text{s}^{-1}\right) = \sum\left(\frac{MAC_{aqSOA} \times I_\lambda \times 10^4 \times \Delta\lambda}{N_A}\right). \quad (3)$$

Here, I_λ is the actinic flux (photons $\text{cm}^{-2}\,\text{s}^{-1}\,\text{nm}^{-1}$) at midday in Davis on the winter solstice from the Tropospheric Ultraviolet and Visible (TUV) Radiation Model version 5.3 (Fig. S1), $\Delta\lambda$ is the interval between TUV wavelengths (1 nm), N_A is Avogadro's number, and the factor of 10^4 is converted from m^2 to cm^2. We calculated the first-order rate constant for loss of sunlight absorption by aqSOA during continued reaction as the negative of the slope of a plot of the natural log of R_{abs} versus reaction time. These rate constants were normalized to Davis wintertime solstice conditions to determine k'_{Rabs}, the pseudo-first-order rate constant for the loss of sunlight absorption by aqSOA. From this we calculated the lifetime for aqSOA sunlight absorption under our experimental conditions using Eq. (4):

$$\tau_{BrC,exp} = \frac{1}{k'_{Rabs}}. \quad (4)$$

This is the timescale for the loss of sunlight absorption during continued illumination, which we refer to as the lifetime of light absorption by brown carbon or, more simply, the lifetime of brown carbon. To extrapolate these calculated lifetimes of aqSOA BrC light absorbance from laboratory to ambient oxidant conditions, we first calculated the value of $\frac{[\bullet H]_{ambient}}{[\bullet H]_{exp}}$, which is the ambient-to-lab ratio of $^\bullet$OH concentration, and the analogous ratio for $^3C^*$. We then multiplied k'_{Rabs} by this ratio to determine $\tau_{BrC,ambient}$, the pseudo-first-order rate constant for loss of BrC absorbance due to that oxidant under ambient conditions. Aqueous concentrations of $^\bullet$OH and $^3C^*$ were taken from Ma et al. (2024) based on measurements of extracts from four different types of particles (winter–spring, summer–fall, fresh wildfire, and aged wildfire) from Davis, California, and including mass transport of gas-phase $^\bullet$OH. We calculated BrC lifetimes for two conditions: cloud/fog drops and aerosol liquid water (ALW), with PM mass / water mass ratios of 3×10^{-5} and 1 µg of PM/µg of water, respectively. Average aqueous oxidant concentrations ($\pm 1\sigma$) were $[^\bullet OH] = 7.6\ (\pm 4.3) \times 10^{-15}$ M for cloud and fog drops and $6.8\ (\pm 1.9) \times 10^{-15}$ M for ALW and $[^3C^*] = 3.6\ (\pm 2.6) \times 10^{-14}$ M for cloud/fog drops and $5.8\ (\pm 3.9) \times 10^{-13}$ M for ALW. We also calculated the overall ambient lifetime of brown carbon with respect to both $^\bullet$OH and $^3C^*$ under these two conditions using Eq. (5):

$$\tau_{BrC,ambient} = \frac{1}{k'_{Rabs,OH} + k'_{Rabs,3C*}}. \quad (5)$$

3 Results and discussion

3.1 Aqueous phenol oxidation by $^\bullet$OH and $^3C^*$

In each experiment, we measured both the aqueous oxidation of ArOH and changes in light absorption by the reaction mixture. As illustrated in Fig. 1, the photooxidation of each phenol follows pseudo-first-order kinetics, with rate constants for phenol loss (k'_{ArOH}) in the range of (1.2–4.1) $\times 10^{-4}\ s^{-1}$ for $^\bullet$OH experiments (Table S3) and (0.19–2.4) $\times 10^{-4}\ s^{-1}$ for $^3C^*$ experiments (Table S4). Differences in kinetics were largely driven by starting conditions, such as initial reactant and oxidant concentrations and small changes in lamp intensity (see j_{2NB} values in Tables S3 and S4). We used k'_{ArOH} values to estimate the steady-state concentration of oxidant in each solution (Sect. 2.3). As shown in Table 1, concentrations of $^\bullet$OH were in the range of (6.5 to 18) $\times 10^{-15}$ M, similar to the typical [$^\bullet$OH] range in cloud/fog drops and ALW (Kaur et al., 2019a; Ma et al., 2023). For $^3C^*$, our experimental concentrations were (1.2–11) $\times 10^{-14}$ M, in the range of cloud/fog drops but lower than the average ALW value of roughly 10^{-13} M described in Sect. 2.4 (Ma et al., 2023).

Each of the parent phenols has an absorption peak between 260 and 290 nm, but only FA, SyrAcid, and SA have any significant absorbance above 300 nm (Fig. S3). These three phenols undergo direct photodegradation (Ma et al., 2021), which accounted for 6 %–35 % of ArOH loss (Fig. S3) and might be a source of light-absorbing products in our experiments. The amount of light absorption by the reaction mixture after illumination varies significantly between different solutions (Figs. S5 and S6). General trends of absorption by phenolic reaction mixtures throughout the course of illumination vary, but there is always more absorption at longer wavelengths compared to the starting phenol. Oxidant type also impacts light absorbance by the aqSOA: after the initial time point, continued $^\bullet$OH oxidation generally decreases absorbance below wavelengths of 300 nm but increases absorbance above 300 nm (Figs. 1 and S5), while $^3C^*$ oxidation mostly increases absorbance across all wavelengths (Figs. 1 and S6).

3.2 Mass absorption coefficients (MACs)

To compare light absorption by aqSOA as a function of phenol, oxidant, and illumination time, we determined mass absorption coefficients (MACs) for each experiment. aqSOA MAC values were determined by correcting measured absorbance values for the contributions from both the remaining starting phenol and the oxidant precursor (Sect. S2). Generally, across tropospherically relevant wavelengths (i.e., above 300 nm), the MAC curves of aqSOA are highest around 300 nm (Figs. 2 and S7) and tail at longer wavelengths. The MAC values of the starting phenols (MAC_{ArOH}) are typically low compared to values of the resulting aqSOA (MAC_{aqSOA}), especially for the first oxidation time

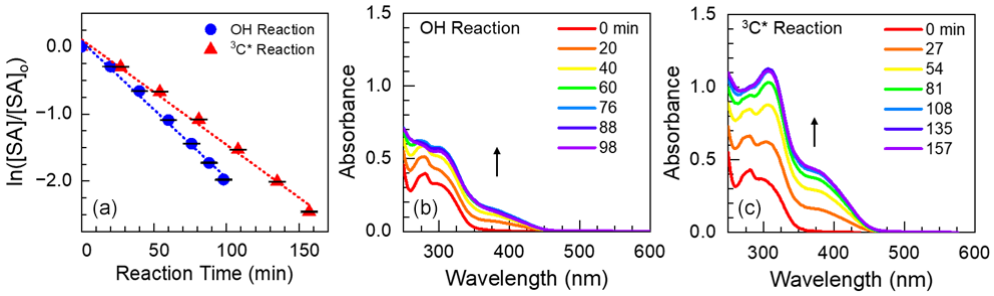

Figure 1. **(a)** Decay kinetics for the loss of syringyl acetone (SA) reacting with •OH (blue circles) or $^3C^*$ (red triangles). Error bars represent 1 standard deviation, estimated from the average relative standard deviations from the corresponding dark controls. Panels **(b)** and **(c)** denote absorbance (in a 5 cm cell) of the reaction mixtures (i.e., oxidant precursor, starting phenol, and products) at various reaction times. Arrows represent the time trends in absorbance.

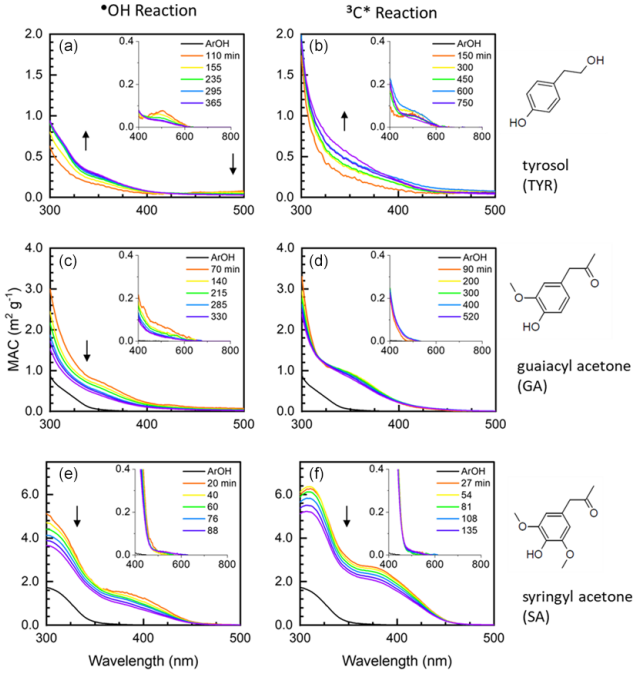

Figure 2. Mass absorption coefficients for aqSOA formed via reactions with •OH **(a, c, e)** and $^3C^*$ **(b, d, f)** for tyrosol (top plots), guaiacyl acetone (middle plots), and syringyl acetone (bottom plots). For a given phenol, each colored line represents a different illumination time (see legend for times). Arrows represent the time trends of aqSOA MAC values after the initial illumination time point. The black line in each panel is the MAC for the parent phenol; the absorbance of the remaining parent phenol was removed from the aqSOA MAC values at each illumination time (Supplement Sect. S2). The MAC for TYR is zero in this wavelength range.

point ($MAC_{aqSOA,t1}$) for both •OH and $^3C^*$ (Table S6). The one exception is FA, which has a high parent absorbance that decreases during oxidation. After the first illumination time point, continued reaction generally decreases light absorbance by the aqSOA, but there are some exceptions (e.g., TYR in Fig. 2 and VAL with $^3C^*$ in Fig. S7).

Figure 2 shows MAC values for three of the phenols we studied – tyrosol, guaiacyl acetone, and syringyl acetone – and their resulting aqSOA. These phenols are substituted versions of the three most abundant phenols from BB: phenol, guaiacol (2-methoxyphenol), and syringol (2,6-dimethoxyphenol). Results for the other three phenols we studied, which are derivatives of guaiacol and syringol, are shown in Fig. S7. For each solution, we first sampled the illumination solution when approximately 25 % of the parent phenol had decayed (i.e., 0.5 $t_{1/2}$), so the corresponding spectrum likely does not capture the maximum absorbance exhibited by the solution. For most of the •OH reactions with the six phenols, the MAC of aqSOA increases from the parent ArOH (which typically has little to no absorbance in the solar wavelengths) to the initial aqSOA. This is because •OH reactions with ArOH form hydroxylated products, which can be important contributors to light absorption (Sun et al., 2010; Yu et al., 2014). Additionally, the formation of quinones, which can contain extensive conjugated pi electrons, might explain our observation of increased aqSOA light absorption at longer wavelengths (Dulo et al., 2021). The aqSOA of TYR is the least absorbing, and aqSOA MAC tends to increase with increased methoxy substitution on the aromatic ring (Figs. 2 and S7). For example, the $MAC_{aqSOA,t1}$ of SyrAcid is greater than that of TYR by a factor of approximately 10 at 300 nm. FA oxidation is somewhat of an exception since the MAC of FA is higher than that of its aqSOA at wavelengths below 350 nm (Fig. S7). The decrease in absorbance during oxidation for FA is probably because of a loss of unsaturation in the acrylic acid substituent, which decreases conjugation and light absorption.

For $^3C^*$ reactions, the trends in absorbance are similar to the •OH results above, including a general increase in MAC from the parent phenol to the initial daughter aqSOA, as shown in Fig. 2 for TYR, GA, and SA (and Fig. S7 for VAL, FA, and SyrAcid). More highly substituted ArOH (FA, SA, and SyrAcid) produce aqSOA that absorbs more strongly compared to the less substituted phenols (TYR, GA, and VAL). Also, $^3C^*$-derived aqSOA absorbs more light

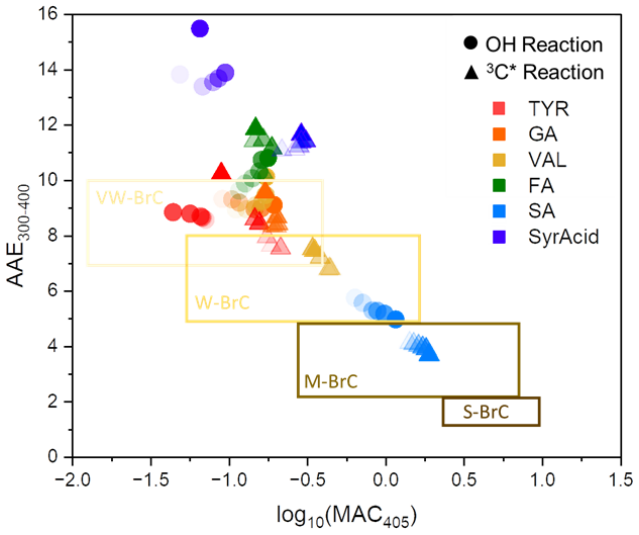

Figure 3. aqSOA light absorption based on the brown carbon (BrC) classification scheme (Saleh, 2020). The boxes from top to bottom represent very weakly absorbing BrC (VW-BrC), weakly absorbing BrC (W-BrC), moderately absorbing BrC (M-BrC), and strongly absorbing BrC (S-BrC). Triangles represent aqSOA formed via reactions of each phenol with the triplet state of DMB, while circles are data from reactions of each phenol with hydroxyl radical. These values are summarized in Table S7 in the Supplement. The time series of each reaction follows a gradient: the first time point is represented as the darkest marker followed by a decrease in color with increasing time.

compared to aqSOA from the corresponding $^{\bullet}$OH reactions. The MAC$_{aqSOA}$ at 300 nm for SyrAcid at this condition was 9.0 m^2 g^{-1}, the highest MAC we observed for both $^{\bullet}$OH and ^{3}C* reactions. One reason for higher MAC values in ^{3}C*-produced aqSOA may be because triplet reactions produce more oligomers, which can strongly absorb light, compared to $^{\bullet}$OH reactions (Yu et al., 2014; Jiang et al., 2021).

In Fig. 3 we plot our MAC data at 405 nm in the BrC classification scheme from Saleh (2020). Most of the phenolic BrC is very weakly absorbing, but the products from SA (our most strongly absorbing aqSOA at 405 nm) are weakly to moderately absorbing. The magnitudes of absorption Ångström exponent (AAE) from 300 to 400 nm (3.7 to 15) and MAC$_{405}$ (0.05 to 1.9) (Table S7) depend on parent ArOH and generally increase with more substituted ArOH. BrC from SA is an exception because the MACs at both 300 and 400 nm are high and do not change drastically across these wavelengths compared to BrC from the other phenols. Oxidant identity also plays an important role in the extent of light absorption by the BrC formed. Most of the BrC formed by $^{\bullet}$OH oxidation was very weakly absorbing, while BrC formed by triplet oxidation had a broader range of absorption, spanning very weakly to moderately absorbing. Also, in most cases, continued oxidation photobleaches BrC towards the very weakly absorbing bin (Fig. 3). Our observation that

Table 1. Oxidant concentrations, pseudo-first-order rate constants for the loss of BrC light absorption (k'_{Rabs}), the total rate of sunlight absorption at the first illumination time point (total $R_{abs,t1}$) for each reaction system, and the fraction of light absorption from 280 to 400 nm.

	$^{\bullet}$OH Reactions				^{3}C* Reactions			
Phenol	$[^{\bullet}OH]_{exp}$ (10^{-15} M)	k'_{Rabs}§ (10^{-3} min^{-1})	Total $R_{abs,t1}$ (10^{-4} mol photon g^{-1} s^{-1})	Fraction of $R_{abs,t1}$ from wavelengths < 400 nm	$[^3C^*]_{exp}$ (10^{-14} M)	k'_{Rabs}§ (10^{-3} min^{-1})	Total $R_{abs,t1}$ (10^{-4} mol photon g^{-1} s^{-1})	Fraction of $R_{abs,t1}$ from wavelengths < 400 nm
Tyrosol (TYR)	8.9	1.0	0.85	0.23	4.0	0.095	0.62	0.37
Guaiacyl acetone (GA)	8.2	3.6	2.0	0.48	2.9	0.50	0.67	0.83
Vanillyl alcohol (VAL)	8.4	4.3	3.1	0.25	1.2	0.17	6.7	0.16
Ferulic acid (FA)	6.5	2.4	2.4	0.67	4.6	0.0053	0.79	0.74
Syringic acid (SyrAcid)	18	9.4	0.70	0.63	11	3.9	2.4	0.64
Syringyl acetone (SA)	17	6.9	4.7	0.69	8.7	2.8	8.2	0.55

most phenolic BrC is very weak to weakly absorbing is consistent with results for water-soluble BrC in ambient particles impacted by residential wood combustion and wildfires (Jiang et al., 2023a; Ma et al., 2024).

3.3 Rates of sunlight absorption

We next calculated R_{abs}, the rate of sunlight absorption, for the parent phenol and resulting aqSOA at each time point, as shown in Fig. 4 for TYR, GA, and SA (and Fig. S8 for VAL, FA, and SyrAcid). Except for FA, the parent phenols generally absorb very weakly at short solar wavelengths (i.e., below 400 nm) or do not absorb any sunlight (i.e., TYR and VAL). As such, the rate of sunlight absorption by aqSOA is generally much higher than that of the parent ArOH, with the exception of FA. For example, going from ArOH to aqSOA, R_{abs} values for GA and SA increase by factors of 14 to 17 for $^{\bullet}$OH reactions and 5.5 to 24 for triplet reactions. The increase for the R_{abs} of SyrAcid aqSOA is much higher, with factors of 74 to 250 for $^{\bullet}$OH and triplet reactions, respectively, due to the very weak absorption by the parent phenol. In contrast, ferulic acid aqSOA shows very small changes compared to FA, with factors of 1.6 for $^{\bullet}$OH reactions and 0.52 for triplet reactions. For the entire set of six phenols, continued oxidation after the first illumination time point can either increase or decrease R_{abs}. For $^{\bullet}$OH reactions, the rate of sunlight absorption for aqSOA from VAL, GA, FA, and SA decreases with increasing oxidation; i.e., continued aging produces less-absorbing aqSOA, possibly because of fragmentation by $^{\bullet}$OH (Sun et al., 2010). Continued ^{3}C* reactions generally decrease R_{abs} for aqSOA but much more slowly than $^{\bullet}$OH reactions. This may be because triplets are less effective at oxidizing aqSOA than is $^{\bullet}$OH (Jiang et al., 2021).

We also calculated the fraction of sunlight absorption due to UV wavelengths, i.e., those below 400 nm. As summarized in Table 1 for the initial time point, the fraction of R_{abs} due to UV wavelengths varies significantly across different ArOH but also, to a smaller extent, across the two oxidants. Fractions of R_{abs} due to UV wavelengths for each illumination time point are shown in Table S7. Generally, more substituted ArOH produce aqSOA where shorter wavelengths dominate sunlight absorption, and this remains throughout the course of reaction. In contrast, for simpler ArOH (i.e., TYR, GA, and VAL), the fraction of R_{abs} due to wavelengths below 400 nm generally increases with reaction time (Table S7). Also, except for VAL, the fraction of R_{abs} contributed by short wavelengths is always higher for the triplet reaction compared to the $^{\bullet}$OH reaction. Interestingly, the VAL–aqSOA formed by both oxidants (Fig. S8, top plot) and TYR–aqSOA by $^{\bullet}$OH (Fig. 4, top plot) contain characteristic peaks at 500 nm, possibly due to quinones. In the case of VAL, this peak behaves differently for the two oxidants. For VAL reaction with $^{\bullet}$OH, aqSOA light absorption diminishes across the entire wavelength range due to photobleaching, with the fastest loss between 400 to 800 nm, possibly due to faster direct photodegradation of chromophores. In contrast, during reactions with triplets, the VAL–aqSOA becomes more absorbing between 300 and 425 nm but photobleaches at longer wavelengths. We observe similar behavior for TYR–aqSOA with $^{\bullet}$OH. This indicates that during the evolution of aqSOA light absorption can simultaneously increase in some wavelength regions and decrease in others.

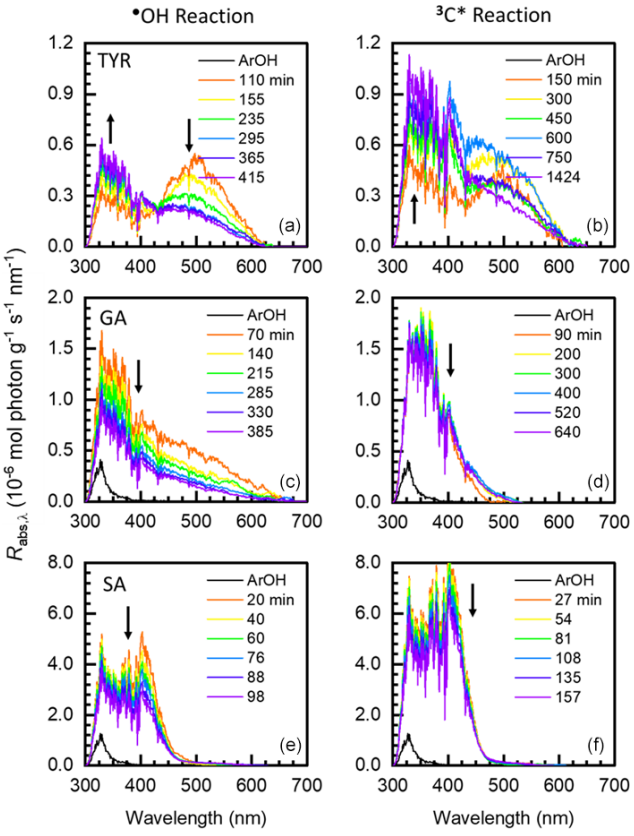

Figure 4. Wavelength-specific rates of sunlight absorption by aqSOA formed via reactions with $^{\bullet}$OH **(a, c, e)** and ^{3}C* **(b, d, f)** for tyrosol (top plots), guaiacyl acetone (middle plots), and syringyl acetone (bottom plots). For a given phenol, the black line represents sunlight absorption by the parent ArOH and colored lines represent absorption for aqSOA at different illumination times (see legend). Arrows represent the time trends of aqSOA MAC values after the initial illumination time point. Rates of aqSOA sunlight absorption for vanillyl alcohol, ferulic acid, and syringic acid are shown in Fig. S8.

3.4 Lifetimes of light-absorbing aqSOA

We calculated the lifetime of light absorption by aqSOA (i.e., the lifetime of phenolic BrC) by monitoring the decline in R_{abs} with continued illumination, as shown in Fig. 5 for SA. We show the equivalent figures for the other five phenols in Figs. S9 and S10. Plotting the natural log of R_{abs} versus reaction time yields the experimental first-order decay rate constant for loss of light absorption ($k'_{Rabs,exp}$). In

some cases, the natural log of R_{abs} increases at short reaction times (e.g., the triplet reactions of TYR, GA, and FA) before decreasing; we did not include these increasing points in our determination of $k'_{Rabs,exp}$. We then normalized this rate constant to Davis midday winter solstice sunlight to obtain (k'_{Rabs}) (Table S8); values are summarized in Table 1. k'_{Rabs} for $^{\bullet}$OH reactions are in the range 1.0 to 9.4 $\times 10^{-3}$ min^{-1}, while rate constants for triplet reactions are lower and range from 0.0053 to 3.9 $\times 10^{-3}$ min^{-1}; i.e., the loss of light-absorbing aqSOA by triplets is much slower than with $^{\bullet}$OH under our experimental conditions. Jiang et al. (2023b) also measured the first-order decay rate constant for loss of light absorption for BrC formed via reactions of GA with $^{\bullet}$OH and ^{3}C*. Compared to their experiments (with no additional oxidant), the rate of decay of ^{3}C*–aqSOA in Jiang et al. (2023b) is higher than our value because their [^{3}C*] is higher by a factor of 3.8. In contrast, for $^{\bullet}$OH–aqSOA, our decay value is higher than that of Jiang et al. (2023) because our [$^{\bullet}$OH] is higher by a factor of 3.2. However, despite these differences in oxidant concentrations, the observed trends for aqSOA are similar. That is, initial photooxidation forms light-absorbing aqSOA, but during extended aging $^{\bullet}$OH–aqSOA photobleaches rapidly, while ^{3}C*–aqSOA photobleaches more slowly. It is possible that molecular differences in the aqSOA formed by ^{3}C* and $^{\bullet}$OH play a role in the different rates of photobleaching. Triplet-mediated reactions efficiently form oligomers, while $^{\bullet}$OH-mediated reactions tend to form hydroxylated products that eventually fragment (Jiang et al., 2023a; Yee et al., 2013). Also, during continuous oxidation triplets are less reactive towards aqSOA, possibly because the BrC molecules do not have phenolic hydroxyl groups or aliphatic double bonds, which are both reactive with triplets (Kaur et al., 2019b; Ma et al., 2021). In contrast, $^{\bullet}$OH, which reacts rapidly with most organic molecules, more quickly degrades phenolic aqSOA.

The inverse of k'_{Rabs} is the lifetime of sunlight absorption by phenolic aqSOA during continued $^{\bullet}$OH and ^{3}C* reactions under our experimental conditions, i.e., the timescale for loss of absorbance by brown carbon compounds in the aqueous SOA. Under our experimental conditions, these BrC lifetimes range from 1.8 to 16 h for $^{\bullet}$OH solutions and 4.3 to 3200 h for ^{3}C* experiments (Fig. S11). Next, we extrapolate these experimental lifetimes to ambient lifetimes by assuming that the concentration of oxidant ($^{\bullet}$OH or ^{3}C*) is driving the loss of brown carbon. We consider two ambient conditions: cloud/fog drops (with a PM mass / liquid water mass ratio of 3×10^{-5} µg of PM/µg of water) and ALW (1 µg of PM/1 µg of water). Concentrations of the two oxidants under our experimental conditions, as well as values for cloud/fog drops and ALW, are described in Tables S9 and S10; the cloud/fog and ALW oxidant concentrations are based on measurements and extrapolations in Ma et al. (2024).

Because the aqueous concentration of $^{\bullet}$OH is similar in our experimental solutions, in cloud/fog drops, and in ALW, we find similar lifetimes for sunlight absorption by aqSOA

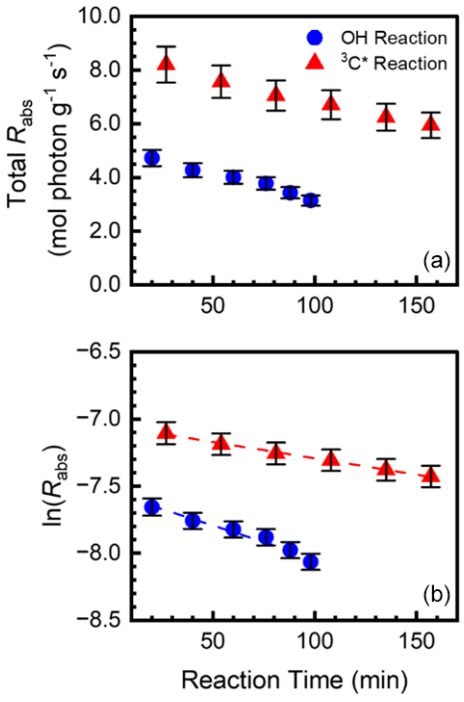

Figure 5. **(a)** Total rate of aqSOA sunlight absorption (R_{abs}, 10^{-4} mol photon g^{-1} s^{-1}) as a function of reaction time during the oxidation of SA by $^{\bullet}$OH (blue circles) and ^{3}C* (red triangles). **(b)** Natural log of R_{abs} versus reaction time, which was used to determine rate constants for the loss of light absorbance by aqSOA. Error bars represent 1 standard deviation propagated from the standard deviations of the dark controls and aqSOA mass yields.

under all three conditions for $^{\bullet}$OH, as shown in Fig. S11. Lifetimes of BrC during reactions in the $^{\bullet}$OH solutions range from 4.2 to 21 h across both ambient conditions for aqSOA from all six highly substituted phenols (Fig. S11). Differences in ArOH substitution do not significantly influence the lifetime of BrC formed from $^{\bullet}$OH, with lifetimes mostly within a factor of 2. Even for TYR–aqSOA, which forms longer-lived absorbing aqSOA, the BrC lifetime only differs by a factor of 4 compared to that for the other phenols. As mentioned above for TYR–aqSOA, this is complicated by the simultaneous occurrence of both photobleaching and photoenhancement in different wavelength regions.

Lifetimes for the light-absorbing aqSOA in the triplet solutions differ from the $^{\bullet}$OH-associated values in two main ways. First, extrapolation to ambient conditions results in a broader range of lifetimes (Fig. S11) due to the 16 times increase in triplet concentrations as we move from cloud/fog drops to particle water. The higher concentration of triplets in ALW makes for shorter lifetimes of light-absorbing aqSOA, ranging from 0.83 to 12 h (except for FA, which is 250 h). However, under cloud/fog conditions, where triplet concentrations are lower, lifetimes of phenolic BrC with respect to triplet reactions are much longer, ranging from 13 to 200 h. The exception again is FA, where the light-absorbing aqSOA

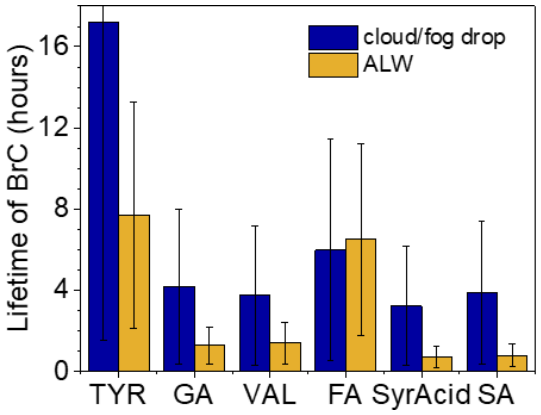

Figure 6. Overall lifetimes of brown carbon (BrC) with respect to photooxidation by $^{\bullet}$OH and ^{3}C* under cloud/fog drop and aerosol liquid water (ALW) conditions calculated using Eq. (5). Lifetimes with respect to photooxidation from the two oxidants individually are shown in Fig. S11. Error bars represent 1 standard deviation, primarily representing the variability in photooxidant concentrations averaged across the four different sample types (Ma et al., 2024), but also include the uncertainty in the rate constant for loss of brown-carbon light absorption.

had a lifetime of 4000 h. This resistance of FA–aqSOA to ^{3}C* oxidation is possibly because a large fraction of FA–aqSOA interactions with triplets result in physical quenching rather than chemical transformation of the aqSOA, likely because the unsaturated side chains from FA undergo isomerization readily (Ma et al., 2021).

We next calculate the overall lifetime of light absorption by phenolic BrC with respect to both $^{\bullet}$OH and ^{3}C* for the two atmospheric conditions. As shown in Fig. 6, for cloud/-fog drops the phenolic BrC lifetimes are typically a few hours but range up to 17 h for TYR aqSOA; these lifetimes are controlled by $^{\bullet}$OH (Fig. S11). In particle water, phenolic BrC lifetimes range from 0.70 to 7.7 h; these are typically shorter than in cloud/fog drops and are generally controlled by reactions with ^{3}C*. The exception is FA, where the lifetimes are controlled by $^{\bullet}$OH, and thus the lifetime is shorter in cloud/-fog drops. While many of the light-absorbing aqSOA lifetimes are under 4 h for the two conditions, the longer lifetimes for brown carbon from TYR and FA show that identity of the precursor phenol also plays a role.

Lastly, we compare the lifetimes of light-absorbing aqSOA across a continuum of liquid water content (LWC), from cloud/fog conditions to ALW (Fig. 7). Combining winter $^{\bullet}$OH and ^{3}C* concentrations as a function of liquid water content from Ma et al. (2023, 2024), we calculated the lifetimes of light-absorbing aqSOA with respect to the two oxidants individually. Lifetimes of phenolic aqSOA with respect to oxidation by $^{\bullet}$OH change relatively little across the enormous range of LWC, a consequence of the predicted small change in hydroxyl radical concentrations (Ma et al., 2023). In contrast, lifetimes of aqSOA produced and oxidized by ^{3}C* show a much larger variation. In the dilute conditions of cloud/fog drops, aqSOA is less susceptible to aging by ^{3}C*, resulting in some of the longer-lived aqSOA across the liquid water content range. But as solutions become more concentrated, the triplet-mediated BrC lifetime drops quickly and then plateaus at a PM mass / water mass ratio of approximately 10^{-2} and above (Fig. 7). This reflects changes in predicted triplet concentrations, which increase by approximately a factor of 16 from cloud/fog to ALW. The net result is that lifetimes of light absorbance by aqSOA are generally controlled by $^{\bullet}$OH under the more dilute conditions of cloud/fog drops, while triplets dominate phenolic BrC lifetimes under more concentrated conditions, including in ALW. The clear exception again is FA, where the BrC lifetime is always controlled by $^{\bullet}$OH, while TYR follows the trend of the other phenols but with a less dramatic shift from $^{\bullet}$OH to ^{3}C* controlling the lifetime as we move from cloud/-fog drops to ALW (Fig. 7). Otherwise, the other four phenols behave as a group, with no clear trend between ArOH substitution and aqSOA lifetime. One caveat to our calculations is that we assume the phenolic BrC lifetimes are governed by reactions with $^{\bullet}$OH and ^{3}C* rather than direct photodegradation. But the latter pathway might also be important, especially for BrC species that absorb at longer wavelengths where the photon flux is higher (Fig. S8). Although it is difficult for us to constrain this, any contribution of direct photodegradation to BrC loss under wintertime Davis conditions would be similar to that in our experimental conditions since our laboratory photon fluxes are similar to ambient values (Fig. S1).

4 Conclusions

We examined light absorption by the aqueous secondary organic aerosol formed from reactions of phenols with two aqueous oxidants: hydroxyl radical ($^{\bullet}$OH) and a triplet excited state (^{3}C*). These two routes are important for ArOH processing and significant contributors to aqSOA formation, but the light absorption trends with continuous reaction had not been evaluated previously. Initial reactions of highly substituted phenols with both oxidants produced aqSOA that absorbs much more sunlight compared to the parent phenol, a result of functionalization and/or oligomerization. Continued photo-aging alters the light absorption by aqSOA. Overall, continued $^{\bullet}$OH oxidation more rapidly causes photobleaching, while the aqSOA formed and oxidized by triplet excited states loses its light absorption much more slowly. Our reactions are restricted with respect to each oxidant; i.e., we did not study how susceptible aqSOA formed by $^{\bullet}$OH is to triplet oxidation or vice versa.

We also extrapolated from our experimental conditions to ambient conditions based on previously measured and estimated ambient oxidant concentrations. Lifetimes of phenolic secondary BrC range from 3.2 to 17 h for cloud/fog drops,

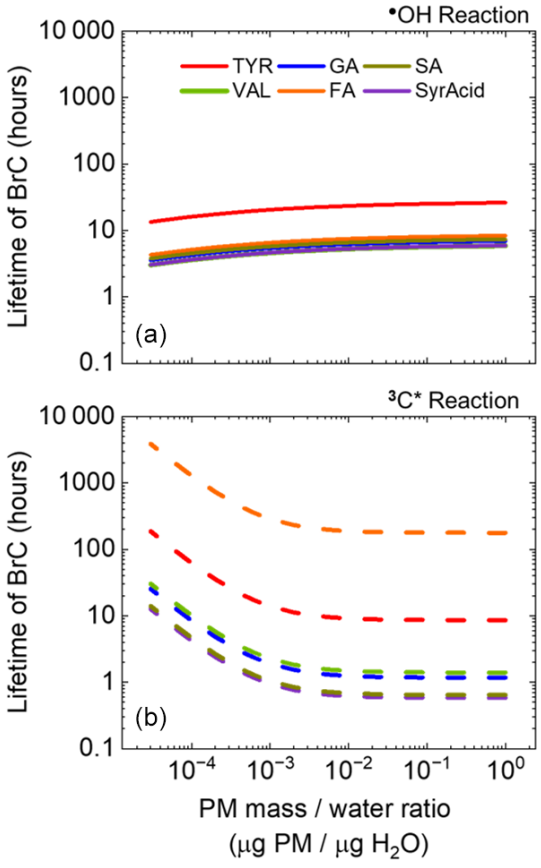

Figure 7. Lifetimes of light-absorbing aqSOA (i.e., BrC) as a function of particle-mass-to-water-mass ratio for TYR (red), GA (blue), SA (mustard), VAL (green), FA (orange), and SyrAcid (purple). Solid and dashed lines indicate lifetimes with respect to reaction with $^{\bullet}$OH **(a)** and ^{3}C* **(b)**, respectively. For a PM concentration of 10 µg m^{-3}, the range of PM mass / water mass ratios corresponds to liquid water contents of 1 to 1×10^{-5} g m^{-3}, i.e., conditions of cloud/fog drops to ALW, respectively.

where $^{\bullet}$OH is the major sink, and from 0.70 to 7.7 for particle water, where triplet excited states are the major sink. Overall, our results will help constrain atmospheric lifetimes of phenolic BrC, which should aid predictions of the global impact of BrC from biomass burning.

Data availability. All data are available upon request.

Supplement. The supplement related to this article is available online at: https://doi.org/10.5194/acp-24-4473-2024-supplement.

Author contributions. CA and SA developed the research goals and designed the experiments. SA and CM performed the $^{\bullet}$OH oxidation experiments, while LM and CG performed the triplet oxidation experiments. SA analyzed the data and prepared the manuscript. CA reviewed and edited the manuscript and provided supervision and oversight during the experiments and writing.

Competing interests. The contact author has declared that none of the authors has any competing interests.

Disclaimer. Publisher's note: Copernicus Publications remains neutral with regard to jurisdictional claims made in the text, published maps, institutional affiliations, or any other geographical representation in this paper. While Copernicus Publications makes every effort to include appropriate place names, the final responsibility lies with the authors.

Acknowledgements. We appreciate the comments and efforts of the four anonymous reviewers.

Financial support. This research has been supported by the National Science Foundation (grant nos. AGS-1649212 and AGS-2220307) and the University of California, Davis (Jastro-Shields Research Award and Donald G. Crosby Fellowship grant).

Review statement. This paper was edited by Theodora Nah and reviewed by four anonymous referees.

References

Aguilera, R., Corringham, T., Gershunov, A., and Benmarhnia, T.: Wildfire smoke impacts respiratory health more than fine particles from other sources: observational evidence from Southern California., Nat. Commun., 12, 1493, https://doi.org/10.1038/s41467-021-21708-0, 2021.

Akagi, S. K., Yokelson, R. J., Wiedinmyer, C., Alvarado, M. J., Reid, J. S., Karl, T., Crounse, J. D., and Wennberg, P. O.: Emission factors for open and domestic biomass burning for use in atmospheric models, Atmos. Chem. Phys., 11, 4039–4072, https://doi.org/10.5194/acp-11-4039-2011, 2011.

Anastasio, C. and McGregor, K. G.: Chemistry of fog waters in California's Central Valley: 1. In situ photoformation of hydroxyl radical and singlet molecular oxygen, Atmos. Environ., 35, 1079–1089, https://doi.org/10.1016/S1352-2310(00)00281-8, 2001.

Andreae, M. O.: Emission of trace gases and aerosols from biomass burning – an updated assessment, Atmos. Chem. Phys., 19, 8523–8546, https://doi.org/10.5194/acp-19-8523-2019, 2019.

Arciva, S., Niedek, C., Mavis, C., Yoon, M., Sanchez, M. E., Zhang, Q., and Anastasio, C.: Aqueous • OH oxidation of highly substituted phenols as a source of secondary organic aerosol, Environ. Sci. Technol., 56, 9959–9967, https://doi.org/10.1021/acs.est.2c02225, 2022.

Berndt, T. and Böge, O.: Gas-phase reaction of OH radicals with phenol, Phys. Chem. Chem. Phys., 5, 342–350, https://doi.org/10.1039/B208187C, 2003.

Bond, T. C., Streets, D. G., Yarber, K. F., Nelson, S. M., Woo, J.-H., and Klimont, Z.: A technology-based global inventory of black and organic carbon emissions from combustion, J. Geophys. Res.-Atmos., 109, D14203, https://doi.org/10.1029/2003JD003697, 2004.

Buxton, G. V., Greenstock, C. L., Helman, W. P., and Ross, A. B.: Critical Review of rate constants for reactions of hydrated electrons, hydrogen atoms and hydroxyl radicals (OH/O- in Aqueous Solution, J. Phys. Chem. Ref. Data, 17, 513–886, https://doi.org/10.1063/1.555805, 1988.

Chang, J. L. and Thompson, J. E.: Characterization of colored products formed during irradiation of aqueous solutions containing H_2O_2 and phenolic compounds, Atmos. Environ., 44, 541–551, https://doi.org/10.1016/j.atmosenv.2009.10.042, 2010.

Coeur-Tourneur, C., Cassez, A., and Wenger, J. C.: Rate coefficients for the gas-phase reaction of hydroxyl radicals with 2-methoxyphenol (guaiacol) and related compounds., J. Phys. Chem. A, 114, 11645–11650, https://doi.org/10.1021/jp1071023, 2010.

Di Lorenzo, R. A., Washenfelder, R. A., Attwood, A. R., Guo, H., Xu, L., Ng, N. L., Weber, R. J., Baumann, K., Edgerton, E., and Young, C. J.: Molecular-Size-Separated Brown Carbon Absorption for Biomass-Burning Aerosol at Multiple Field Sites, Environ. Sci. Technol., 51, 3128–3137, https://doi.org/10.1021/acs.est.6b06160, 2017.

Dulo, B., Phan, K., Githaiga, J., Raes, K., and De Meester, S.: Natural quinone dyes: A review on structure, extraction techniques, analysis and application potential, Waste Biomass Valor., 12, 6339–6374, https://doi.org/10.1007/s12649-021-01443-9, 2021.

Fleming, L. T., Lin, P., Roberts, J. M., Selimovic, V., Yokelson, R., Laskin, J., Laskin, A., and Nizkorodov, S. A.: Molecular composition and photochemical lifetimes of brown carbon chromophores in biomass burning organic aerosol, Atmos. Chem. Phys., 20, 1105–1129, https://doi.org/10.5194/acp-20-1105-2020, 2020.

Garofalo, L. A., Pothier, M. A., Levin, E. J. T., Campos, T., Kreidenweis, S. M., and Farmer, D. K.: Emission and Evolution of Submicron Organic Aerosol in Smoke from Wildfires in the Western United States, ACS Earth Space Chem., 3, 1237–1247, https://doi.org/10.1021/acsearthspacechem.9b00125, 2019.

Graber, E. R. and Rudich, Y.: Atmospheric HULIS: How humic-like are they? A comprehensive and critical review, Atmos. Chem. Phys., 6, 729–753, https://doi.org/10.5194/acp-6-729-2006, 2006.

Grieshop, A. P., Logue, J. M., Donahue, N. M., and Robinson, A. L.: Laboratory investigation of photochemical oxidation of organic aerosol from wood fires 1: measurement and simulation of organic aerosol evolution, Atmos. Chem. Phys., 9, 1263–1277, https://doi.org/10.5194/acp-9-1263-2009, 2009.

Gurol, M. D. and Nekouinaini, S.: Kinetic behavior of ozone in aqueous solutions of substituted phenols, Ind. Eng. Chem. Fund., 23, 54–60, https://doi.org/10.1021/i100013a011, 1984.

Hallquist, M., Wenger, J. C., Baltensperger, U., Rudich, Y., Simpson, D., Claeys, M., Dommen, J., Donahue, N. M., George, C., Goldstein, A. H., Hamilton, J. F., Herrmann, H., Hoffmann, T., Iinuma, Y., Jang, M., Jenkin, M. E., Jimenez, J. L., Kiendler-Scharr, A., Maenhaut, W., McFiggans, G., Mentel, Th. F., Monod, A., Prévôt, A. S. H., Seinfeld, J. H., Surratt, J. D., Szmigielski, R., and Wildt, J.: The formation, properties and impact of secondary organic aerosol: current and emerging issues, Atmos. Chem. Phys., 9, 5155–5236, https://doi.org/10.5194/acp-9-5155-2009, 2009.

Heald, C. L., Henze, D. K., Horowitz, L. W., Feddema, J., Lamarque, J. F., Guenther, A., Hess, P. G., Vitt, F., Seinfeld, J. H., Goldstein, A. H., and Fung, I.: Predicted change in global secondary organic aerosol concentrations in response to future climate, emissions, and land use change, J. Geophys. Res., 113, D05211, https://doi.org/10.1029/2007JD009092, 2008.

Hecobian, A., Zhang, X., Zheng, M., Frank, N., Edgerton, E. S., and Weber, R. J.: Water-Soluble Organic Aerosol material and the light-absorption characteristics of aqueous extracts measured over the Southeastern United States, Atmos. Chem. Phys., 10, 5965–5977, https://doi.org/10.5194/acp-10-5965-2010, 2010.

Hems, R. F., Schnitzler, E. G., Bastawrous, M., Soong, R., Simpson, A. J., and Abbatt, J. P. D.: Aqueous photoreactions of wood smoke brown carbon, ACS Earth Space Chem., 4, 1149–1160, https://doi.org/10.1021/acsearthspacechem.0c00117, 2020.

Hems, R. F., Schnitzler, E. G., Liu-Kang, C., Cappa, C. D., and Abbatt, J. P. D.: Aging of atmospheric brown carbon aerosol, ACS Earth Space Chem., 5, 722–748, https://doi.org/10.1021/acsearthspacechem.0c00346, 2021.

Hennigan, C. J., Miracolo, M. A., Engelhart, G. J., May, A. A., Presto, A. A., Lee, T., Sullivan, A. P., McMeeking, G. R., Coe, H., Wold, C. E., Hao, W.-M., Gilman, J. B., Kuster, W. C., de Gouw, J., Schichtel, B. A., Collett Jr., J. L., Kreidenweis, S. M., and Robinson, A. L.: Chemical and physical transformations of organic aerosol from the photo-oxidation of open biomass burning emissions in an environmental chamber, Atmos. Chem. Phys., 11, 7669–7686, https://doi.org/10.5194/acp-11-7669-2011, 2011.

Huang, D. D., Zhang, Q., Cheung, H. H. Y., Yu, L., Zhou, S., Anastasio, C., Smith, J. D., and Chan, C. K.: Formation and Evolution of aqSOA from Aqueous-Phase Reactions of Phenolic Carbonyls: Comparison between Ammonium Sulfate and Ammonium Nitrate Solutions., Environ. Sci. Technol., 52, 9215–9224, https://doi.org/10.1021/acs.est.8b03441, 2018.

Jiang, W., Misovich, M. V., Hettiyadura, A. P. S., Laskin, A., McFall, A. S., Anastasio, C., and Zhang, Q.: Photosensitized Reactions of a Phenolic Carbonyl from Wood Combustion in the Aqueous Phase-Chemical Evolution and Light Absorption Properties of AqSOA, Environ. Sci. Technol., 55, 5199–5211, https://doi.org/10.1021/acs.est.0c07581, 2021.

Jiang, W., Ma, L., Niedek, C., Anastasio, C., and Zhang, Q.: Chemical and Light-Absorption Properties of Water-Soluble Organic Aerosols in Northern California and Photooxidant Production by Brown Carbon Components, ACS Earth Space Chem., 7, 1107–1119, https://doi.org/10.1021/acsearthspacechem.3c00022, 2023a.

Jiang, W., Niedek, C., Anastasio, C., and Zhang, Q.: Photoaging of phenolic secondary organic aerosol in the aqueous phase: evolution of chemical and optical properties and effects of oxidants, Atmos. Chem. Phys., 23, 7103–7120, https://doi.org/10.5194/acp-23-7103-2023, 2023b.

Jimenez, J. L., Canagaratna, M. R., Donahue, N. M., Prevot, A. S. H., Zhang, Q., Kroll, J. H., DeCarlo, P. F., Allan, J. D., Coe, H., Ng, N. L., Aiken, A. C., Docherty, K. S., Ulbrich, I. M., Grieshop, A. P., Robinson, A. L., Duplissy, J., Smith, J. D., Wilson, K. R., Lanz, V. A., Hueglin, C., Sun, Y. L., Tian, J.,

Laaksonen, A., Raatikainen, T., Rautiainen, J., Vaattovaara, P., Ehn, M., Kulmala, M., Tomlinson, J. M., Collins, D. R., Cubison, M. J., Dunlea, E. J., Huffman, J. A., Onasch, T. B., Alfarra, M. R., Williams, P. I., Bower, K., Kondo, Y., Schneider, J., Drewnick, F., Borrmann, S., Weimer, S., Demerjian, K., Salcedo, D., Cottrell, L., Griffin, R., Takami, A., Miyoshi, T., Hatakeyama, S., Shimono, A., Sun, J. Y., Zhang, Y. M., Dzepina, K., Kimmel, J. R., Sueper, D., Jayne, J. T., Herndon, S. C., Trimborn, A. M., Williams, L. R., Wood, E. C., Middlebrook, A. M., Kolb, C. E., Baltensperger, U., and Worsnop, D. R.: Evolution of organic aerosols in the atmosphere, Science, 326, 1525–1529, https://doi.org/10.1126/science.1180353, 2009.

Jo, D. S., Park, R. J., Lee, S., Kim, S.-W., and Zhang, X.: A global simulation of brown carbon: implications for photochemistry and direct radiative effect, Atmos. Chem. Phys., 16, 3413–3432, https://doi.org/10.5194/acp-16-3413-2016, 2016.

Kaeswurm, J. A. H., Scharinger, A., Teipel, J., and Buchweitz, M.: Absorption coefficients of phenolic structures in different solvents routinely used for experiments, Molecules, 26, 4656, https://doi.org/10.3390/molecules26154656, 2021.

Kanakidou, M., Seinfeld, J. H., Pandis, S. N., Barnes, I., Dentener, F. J., Facchini, M. C., Van Dingenen, R., Ervens, B., Nenes, A., Nielsen, C. J., Swietlicki, E., Putaud, J. P., Balkanski, Y., Fuzzi, S., Horth, J., Moortgat, G. K., Winterhalter, R., Myhre, C. E. L., Tsigaridis, K., Vignati, E., Stephanou, E. G., and Wilson, J.: Organic aerosol and global climate modelling: a review, Atmos. Chem. Phys., 5, 1053–1123, https://doi.org/10.5194/acp-5-1053-2005, 2005.

Kaur, R., Labins, J. R., Helbock, S. S., Jiang, W., Bein, K. J., Zhang, Q., and Anastasio, C.: Photooxidants from brown carbon and other chromophores in illuminated particle extracts, Atmos. Chem. Phys., 19, 6579–6594, https://doi.org/10.5194/acp-19-6579-2019, 2019a.

Kaur, R., Hudson, B. M., Draper, J., Tantillo, D. J., and Anastasio, C.: Aqueous reactions of organic triplet excited states with atmospheric alkenes, Atmos. Chem. Phys., 19, 5021–5032, https://doi.org/10.5194/acp-19-5021-2019, 2019b.

Kim, K.-H., Kabir, E., and Kabir, S.: A review on the human health impact of airborne particulate matter, Environ. Int., 74, 136–143, https://doi.org/10.1016/j.envint.2014.10.005, 2015.

Kirchstetter, T. W. and Thatcher, T. L.: Contribution of organic carbon to wood smoke particulate matter absorption of solar radiation, Atmos. Chem. Phys., 12, 6067–6072, https://doi.org/10.5194/acp-12-6067-2012, 2012.

Kleinman, L. I., Sedlacek III, A. J., Adachi, K., Buseck, P. R., Collier, S., Dubey, M. K., Hodshire, A. L., Lewis, E., Onasch, T. B., Pierce, J. R., Shilling, J., Springston, S. R., Wang, J., Zhang, Q., Zhou, S., and Yokelson, R. J.: Rapid evolution of aerosol particles and their optical properties downwind of wildfires in the western US, Atmos. Chem. Phys., 20, 13319–13341, https://doi.org/10.5194/acp-20-13319-2020, 2020.

Laskin, A., Laskin, J., and Nizkorodov, S. A.: Chemistry of atmospheric brown carbon, Chem. Rev., 115, 4335–4382, https://doi.org/10.1021/cr5006167, 2015.

Liu, D., Li, S., Hu, D., Kong, S., Cheng, Y., Wu, Y., Ding, S., Hu, K., Zheng, S., Yan, Q., Zheng, H., Zhao, D., Tian, P., Ye, J., Huang, M., and Ding, D.: Evolution of Aerosol Optical Properties from Wood Smoke in Real Atmosphere Influenced by Burning Phase and Solar Radiation, Environ. Sci. Technol., 55, 5677–5688, https://doi.org/10.1021/acs.est.0c07569, 2021.

Li, X., Tao, Y., Zhu, L., Ma, S., Luo, S., Zhao, Z., Sun, N., Ge, X., and Ye, Z.: Optical and chemical properties and oxidative potential of aqueous-phase products from OH and $^3C^*$-initiated photooxidation of eugenol, Atmos. Chem. Phys., 22, 7793–7814, https://doi.org/10.5194/acp-22-7793-2022, 2022.

Li, Y. J., Huang, D. D., Cheung, H. Y., Lee, A. K. Y., and Chan, C. K.: Aqueous-phase photochemical oxidation and direct photolysis of vanillin – a model compound of methoxy phenols from biomass burning, Atmos. Chem. Phys., 14, 2871–2885, https://doi.org/10.5194/acp-14-2871-2014, 2014.

Ma, L., Guzman, C., Niedek, C., Tran, T., Zhang, Q. and Anastasio, C.: Kinetics and mass yields of aqueous secondary organic aerosol from highly substituted phenols reacting with a triplet excited state, Environ. Sci. Technol., 55, 5772–5781, https://doi.org/10.1021/acs.est.1c00575, 2021.

Ma, L., Worland, R., Jiang, W., Niedek, C., Guzman, C., Bein, K. J., Zhang, Q., and Anastasio, C.: Predicting photooxidant concentrations in aerosol liquid water based on laboratory extracts of ambient particles, Atmos. Chem. Phys., 23, 8805–8821, https://doi.org/10.5194/acp-23-8805-2023, 2023.

Ma, L., Worland, R., Heinlein, L., Guzman, C., Jiang, W., Niedek, C., Bein, K. J., Zhang, Q., and Anastasio, C.: Seasonal variations in photooxidant formation and light absorption in aqueous extracts of ambient particles, Atmos. Chem. Phys., 24, 1–21, https://doi.org/10.5194/acp-24-1-2024, 2024.

McFall, A. S., Johnson, A. W., and Anastasio, C.: Air-Water Partitioning of Biomass-Burning Phenols and the Effects of Temperature and Salinity, Environ. Sci. Technol., 54, 3823–3830, https://doi.org/10.1021/acs.est.9b06443, 2020.

Misovich, M. V., Hettiyadura, A. P. S., Jiang, W., Zhang, Q., and Laskin, A.: Molecular-Level Study of the Photo-Oxidation of Aqueous-Phase Guaiacyl Acetone in the Presence of $^3C^*$: Formation of Brown Carbon Products, ACS Earth Space Chem., https://doi.org/10.1021/acsearthspacechem.1c00103, 2021.

O'Dell, K., Bilsback, K., Ford, B., Martenies, S. E., Magzamen, S., Fischer, E. V., and Pierce, J. R.: Estimated mortality and morbidity attributable to smoke plumes in the united states: not just a western US problem, GeoHealth, 5, e2021GH000457, https://doi.org/10.1029/2021GH000457, 2021.

Ortega, A. M., Day, D. A., Cubison, M. J., Brune, W. H., Bon, D., de Gouw, J. A., and Jimenez, J. L.: Secondary organic aerosol formation and primary organic aerosol oxidation from biomass-burning smoke in a flow reactor during FLAME-3, Atmos. Chem. Phys., 13, 11551–11571, https://doi.org/10.5194/acp-13-11551-2013, 2013.

Palm, B. B., Peng, Q., Fredrickson, C. D., Lee, B. H., Garofalo, L. A., Pothier, M. A., Kreidenweis, S. M., Farmer, D. K., Pokhrel, R. P., Shen, Y., Murphy, S. M., Permar, W., Hu, L., Campos, T. L., Hall, S. R., Ullmann, K., Zhang, X., Flocke, F., Fischer, E. V., and Thornton, J. A.: Quantification of organic aerosol and brown carbon evolution in fresh wildfire plumes, P. Natl. Acad. Sci. USA, 117, 29469–29477, https://doi.org/10.1073/pnas.2012218117, 2020.

Powelson, M. H., Espelien, B. M., Hawkins, L. N., Galloway, M. M., and De Haan, D. O.: Brown carbon formation by aqueous-phase carbonyl compound reactions with amines

and ammonium sulfate, Environ. Sci. Technol., 48, 985–993, https://doi.org/10.1021/es4038325, 2014.

Reid, J. S., Koppmann, R., Eck, T. F., and Eleuterio, D. P.: A review of biomass burning emissions part II: intensive physical properties of biomass burning particles, Atmos. Chem. Phys., 5, 799–825, https://doi.org/10.5194/acp-5-799-2005, 2005.

Robinson, A. L., Donahue, N. M., Shrivastava, M. K., Weitkamp, E. A., Sage, A. M., Grieshop, A. P., Lane, T. E., Pierce, J. R., and Pandis, S. N.: Rethinking organic aerosols: semivolatile emissions and photochemical aging., Science, 315, 1259–1262, https://doi.org/10.1126/science.1133061, 2007.

Saleh, R.: From Measurements to Models: Toward Accurate Representation of Brown Carbon in Climate Calculations, Curr. Pollut. Reports, 6, 90–104, https://doi.org/10.1007/s40726-020-00139-3, 2020.

Saleh, R., Hennigan, C. J., McMeeking, G. R., Chuang, W. K., Robinson, E. S., Coe, H., Donahue, N. M., and Robinson, A. L.: Absorptivity of brown carbon in fresh and photo-chemically aged biomass-burning emissions, Atmos. Chem. Phys., 13, 7683–7693, https://doi.org/10.5194/acp-13-7683-2013, 2013.

Schauer, J. J., Kleeman, M. J., Cass, G. R., and Simoneit, B. R.: Measurement of emissions from air pollution sources. 3. C1-C29 organic compounds from fireplace combustion of wood, Environ. Sci. Technol., 35, 1716–1728, https://doi.org/10.1021/es001331e, 2001.

Schnitzler, E. G., Gerrebos, N. G. A., Carter, T. S., Huang, Y., Heald, C. L., Bertram, A. K., and Abbatt, J. P. D.: Rate of atmospheric brown carbon whitening governed by environmental conditions, P. Natl. Acad. Sci. USA, 119, e2205610119, https://doi.org/10.1073/pnas.2205610119, 2022.

Shrivastava, M., Cappa, C. D., Fan, J., Goldstein, A. H., Guenther, A. B., Jimenez, J. L., Kuang, C., Laskin, A., Martin, S. T., Ng, N. L., Petaja, T., Pierce, J. R., Rasch, P. J., Roldin, P., Seinfeld, J. H., Shilling, J., Smith, J. N., Thornton, J. A., Volkamer, R., Wang, J., Worsnop, D. R., Zaveri, R. A., Zelenyuk, A., and Zhang, Q.: Recent advances in understanding secondary organic aerosol: Implications for global climate forcing, Rev. Geophys., 55, 509–559, https://doi.org/10.1002/2016RG000540, 2017.

Smith, J. D., Kinney, H., and Anastasio, C.: Aqueous benzene-diols react with an organic triplet excited state and hydroxyl radical to form secondary organic aerosol, Phys. Chem. Chem. Phys., 17, 10227–10237, https://doi.org/10.1039/c4cp06095d, 2015.

Smith, J. D., Kinney, H., and Anastasio, C.: Phenolic carbonyls undergo rapid aqueous photodegradation to form low-volatility, light-absorbing products, Atmos. Environ., 126, 36–44, https://doi.org/10.1016/j.atmosenv.2015.11.035, 2016.

Sun, Y. L., Zhang, Q., Anastasio, C., and Sun, J.: Insights into secondary organic aerosol formed via aqueous-phase reactions of phenolic compounds based on high resolution mass spectrometry, Atmos. Chem. Phys., 10, 4809–4822, https://doi.org/10.5194/acp-10-4809-2010, 2010.

Volkamer, R., Jimenez, J. L., San Martini, F., Dzepina, K., Zhang, Q., Salcedo, D., Molina, L. T., Worsnop, D. R., and Molina, M. J.: Secondary organic aerosol formation from anthropogenic air pollution: Rapid and higher than expected, Geophys. Res. Lett., 33, L17811, https://doi.org/10.1029/2006GL026899, 2006.

Wang, Y., Huang, W., Tian, L., Wang, Y., Li, F., Huang, D. D., Zhang, R., Go Mabato, B. R., Huang, R.-J., Chen, Q., Ge, X., Du, L., Ma, Y. G., Gen, M., Hoi, K. I., Mok, K. M., Yu, J. Z., Chan, C. K., Li, X., and Li, Y. J.: Decay Kinetics and Absorption Changes of Methoxyphenols and Nitrophenols during Nitrate-Mediated Aqueous Photochemical Oxidation at 254 and 313 nm, ACS Earth Space Chem., 6, 1115–1125, https://doi.org/10.1021/acsearthspacechem.2c00021, 2022.

Yee, L. D., Kautzman, K. E., Loza, C. L., Schilling, K. A., Coggon, M. M., Chhabra, P. S., Chan, M. N., Chan, A. W. H., Hersey, S. P., Crounse, J. D., Wennberg, P. O., Flagan, R. C., and Seinfeld, J. H.: Secondary organic aerosol formation from biomass burning intermediates: phenol and methoxyphenols, Atmos. Chem. Phys., 13, 8019–8043, https://doi.org/10.5194/acp-13-8019-2013, 2013.

Yu, L., Smith, J., Laskin, A., Anastasio, C., Laskin, J., and Zhang, Q.: Chemical characterization of SOA formed from aqueous-phase reactions of phenols with the triplet excited state of carbonyl and hydroxyl radical, Atmos. Chem. Phys., 14, 13801–13816, https://doi.org/10.5194/acp-14-13801-2014, 2014.

Yu, L., Smith, J., Laskin, A., George, K. M., Anastasio, C., Laskin, J., Dillner, A. M., and Zhang, Q.: Molecular transformations of phenolic SOA during photochemical aging in the aqueous phase: competition among oligomerization, functionalization, and fragmentation, Atmos. Chem. Phys., 16, 4511–4527, https://doi.org/10.5194/acp-16-4511-2016, 2016.

Zhang, A., Wang, Y., Zhang, Y., Weber, R. J., Song, Y., Ke, Z., and Zou, Y.: Modeling the global radiative effect of brown carbon: a potentially larger heating source in the tropical free troposphere than black carbon, Atmos. Chem. Phys., 20, 1901–1920, https://doi.org/10.5194/acp-20-1901-2020, 2020.

Zhao, R., Lee, A. K. Y., Huang, L., Li, X., Yang, F., and Abbatt, J. P. D.: Photochemical processing of aqueous atmospheric brown carbon, Atmos. Chem. Phys., 15, 6087–6100, https://doi.org/10.5194/acp-15-6087-2015, 2015.

Zhong, M. and Jang, M.: Dynamic light absorption of biomass-burning organic carbon photochemically aged under natural sunlight, Atmos. Chem. Phys., 14, 1517–1525, https://doi.org/10.5194/acp-14-1517-2014, 2014.

Zhou, X., Josey, K., Kamareddine, L., Caine, M. C., Liu, T., Mickley, L. J., Cooper, M., and Dominici, F.: Excess of COVID-19 cases and deaths due to fine particulate matter exposure during the 2020 wildfires in the United States, Sci. Adv., 7, eabi8789, https://doi.org/10.1126/sciadv.abi8789, 2021.

Supplement of Atmos. Chem. Phys., 24, 4473–4485, 2024
https://doi.org/10.5194/acp-24-4473-2024-supplement

Atmospheric Chemistry and Physics
Open Access
EGU

Supplement of

Formation and loss of light absorbance by phenolic aqueous SOA by $^{\cdot}$OH and an organic triplet excited state

Stephanie Arciva et al.

Correspondence to: Cort Anastasio (canastasio@ucdavis.edu)

Table of Contents

Table S1. Sampling time for ArOH oxidation reactions. Reaction times indicate approximately one, two, and three half-lives (i.e., $t_{1/2}$, $2t_{1/2}$, and $3t_{1/2}$) unless noted otherwise. ArOH concentrations were 100 μM except as marked. For $^{\bullet}$OH reactions, the H_2O_2 concentration was 5 mM, except for FA, SyrAcid and SA, which had 10 mM H_2O_2. For ^{3}C* reactions, solutions contained 10 μM DMB, except for tyrosol, which had 5 μM DMB.

Reaction Condition	$^{\bullet}$OH Reaction (min)	^{3}C* Reaction (min)
Tyrosol (TYR)	110	150
$t_{1/2}$	155	300
	235	450
2 $t_{1/2}$	295	600 ($0.85t_{1/2}$)
	365	750
3 $t_{1/2}$	415	1424 ($2t_{1/2}$)
Guaiacylacetone (GA)	70	90
$t_{1/2}$	140	200
	215	300
2 $t_{1/2}$	285	400
	330	520
3 $t_{1/2}$	385	640
Vanillyl alcohol (VAL)	60	90
$t_{1/2}$	143	130
	193	250
2 $t_{1/2}$	258	432
	323	610
3 $t_{1/2}$	378	1184 ($3.4t_{1/2}$)
Ferulic acid (FA) (50 μM)	60	120
$t_{1/2}$	140	240 ($0.43t_{1/2}$)
	210	440
2 $t_{1/2}$	280	680 ($1.6t_{1/2}$)
	350	-
3 $t_{1/2}$	420	1170 ($3.8t_{1/2}$)
Syringic acid (SyrAcid) (50 μM)	20	24
$t_{1/2}$	45	48
	70	72
2 $t_{1/2}$	85	96
	100	119
3 $t_{1/2}$	120	131
Syringylacetone (SA) (50 μM)	20	27
$t_{1/2}$	40	54
	60	81
2 $t_{1/2}$	76	108 ($2.2t_{1/2}$)
	88	135
3 $t_{1/2}$	98	157 ($3.5t_{1/2}$)

Table S2. Molar absorptivities for highly substituted ArOH. Base-10 molar absorption coefficients (ε) for aqueous ArOH determined from five different solutions of ArOH (25 μM, 100 μM, 500 μM, 1.0 mM, and 2.0 mM) in a 1 cm cell. Plots are shown in Figure S4.

Wave-length (nm)	TYR	GA	VAL	*trans*-FA [a]		*cis*-FA [a]		SyrAcid [b]		SA
				pH 5	pH 2	pH 5	pH 2	pH 5	pH 2	
200	12500	36200	43900	11500	8460	18400	15900	24000	15500	44200
201	9690	35400	43200	11600	8350	18300	15700	24300	15900	45200
202	7890	33400	40000	11700	8170	18300	15000	24900	16700	46600
203	7030	30700	37300	11800	7990	18400	14300	25500	17400	47300
204	6240	27700	33600	12000	7840	18500	13700	26300	18200	47500
205	5790	24200	29300	12200	7730	18800	13000	27000	19100	46700
206	5540	21100	24600	12500	7650	18900	12400	27700	19900	45100
207	5490	18400	20400	12800	7640	18900	11800	28200	20700	42700
208	5490	16000	16500	13200	7680	18900	11200	28700	21500	39800
209	5560	14100	13300	13600	7820	18900	10800	29100	22200	36500
210	5640	12600	10700	14100	8020	18900	10500	29300	22900	33300
211	5750	11300	8960	14500	8260	18800	10200	29400	23600	30300
212	5910	10400	7710	14900	8500	18600	10000	29500	24200	27500
213	6010	9630	6940	15200	8750	18500	9890	29600	24800	25100
214	6090	9050	6450	15500	9000	18300	9720	29400	25200	22900
215	6200	8580	6170	15700	9220	18000	9570	29200	25600	21000
216	6290	8180	6010	15900	9390	17600	9430	28700	25900	19400
217	6470	7860	5950	15900	9520	17200	9270	27900	26100	18000
218	6630	7590	5960	15800	9590	16700	9090	26900	26000	16900
219	6830	7350	6010	15700	9550	16200	8920	25600	25700	15900
220	6970	7160	6070	15300	9400	15600	8740	23500	25100	15000
221	7030	6970	6150	14900	9130	15000	8550	21800	24200	14300
222	7000	6800	6240	14500	8800	14400	8340	20100	23000	13600
223	6800	6640	6340	14100	8490	13800	8130	18000	21500	13000
224	6510	6480	6430	13800	8280	13200	7960	15600	19600	12500
225	6050	6330	6520	13700	8150	12600	7830	14100	17500	12100
226	5470	6180	6590	13600	8100	12100	7720	11800	15300	11700
227	4820	6030	6630	13600	8150	11600	7630	10200	13100	11300
228	4160	5880	6620	13600	8250	11100	7550	8150	11100	10900
229	3560	5710	6560	13500	8370	10700	7490	7080	9370	10600
230	2910	5520	6430	13500	8510	10300	7410	6180	7590	10200
231	2320	5290	6230	13400	8650	9910	7350	5450	6240	9870
232	1790	5040	5980	13200	8750	9520	7280	4880	5130	9530

wave length (nm)	TYR	GA	VAL	*trans*-FA		*cis*-FA		SyrAcid		SA
				pH 5	pH 2	pH 5	pH 2	pH 5	pH 2	
233	1390	4760	5670	13000	8830	9160	7190	4450	4230	9160
234	1070	4480	5300	12800	8860	8830	7090	4130	3460	8770
235	800	4170	4890	12600	8860	8510	6980	3900	2920	8350
236	605	3850	4450	12300	8830	8210	6860	3740	2510	7920
237	450	3520	3920	12000	8780	7920	6730	3650	2200	7480
238	344	3200	3450	11700	8710	7640	6590	3610	2000	7010
239	266	2890	3000	11400	8640	7410	6450	3630	1880	6520
240	208	2580	2550	11000	8550	7210	6300	3700	1820	6050
241	171	2300	2140	10600	8440	7050	6140	3820	1820	5590
242	146	2050	1750	10200	8300	6930	5980	3970	1870	5110
243	132	1810	1430	9730	8120	6830	5800	4170	1960	4650
244	125	1620	1140	9270	7900	6780	5630	4380	2080	4230
245	124	1450	925	8700	7640	6780	5440	4630	2240	3830
246	129	1310	752	8240	7360	6800	5240	4900	2410	3470
247	137	1190	619	7780	7040	6840	5060	5180	2610	3150
248	149	1090	517	7330	6690	6930	4870	5480	2840	2840
249	163	1010	445	6910	6320	7040	4700	5790	3080	2570
250	182	947	399	6510	5950	7160	4530	6090	3330	2350
251	203	895	372	6160	5560	7320	4350	6410	3610	2150
252	226	855	361	5860	5070	7490	4280	6710	3950	1980
253	258	827	363	5610	4690	7680	4100	7030	4270	1840
254	289	810	377	5410	4320	7890	3950	7330	4600	1720
255	327	804	402	5280	3990	8120	3840	7630	4950	1630
256	367	810	437	5210	3690	8370	3740	7900	5320	1550
257	416	827	480	5210	3460	8610	3670	8140	5700	1480
258	468	856	533	5270	3270	8860	3630	8370	6090	1440
259	524	897	596	5400	3130	9090	3610	8550	6480	1420
260	583	949	667	5590	3060	9290	3620	8710	6870	1410
261	645	1010	747	5820	3040	9480	3640	8830	7250	1410
262	711	1080	835	6100	3060	9650	3680	8900	7750	1430
263	785	1170	933	6440	3120	9810	3760	8920	8120	1450
264	862	1270	1040	6810	3230	9930	3850	8910	8480	1480
265	944	1370	1150	7210	3370	10000	3920	8850	8810	1520
266	1030	1480	1260	7630	3540	10100	4020	8760	9090	1560
267	1100	1590	1400	8060	3730	10200	4140	8630	9350	1610
268	1180	1710	1520	8490	3960	10200	4260	8470	9590	1640
269	1240	1830	1650	8850	4190	10100	4390	8280	9790	1680
270	1300	1950	1770	9270	4440	10100	4490	8080	9960	1710
271	1360	2080	1890	9720	4710	9940	4590	7860	10000	1740
272	1420	2200	2020	10200	4990	9790	4670	7620	10100	1770

wave length (nm)	TYR	GA	VAL	*trans*-FA		*cis*-FA		SyrAcid		SA
				pH 5	pH 2	pH 5	pH 2	pH 5	pH 2	
273	1480	2320	2140	10600	5420	9580	4770	7360	10200	1780
274	1530	2440	2260	11100	5730	9350	4890	7100	10200	1790
275	1570	2550	2370	11500	6050	9100	5020	6840	10200	1800
276	1570	2660	2460	11900	6380	8850	5140	6570	10200	1800
277	1540	2750	2520	12300	6730	8610	5240	6310	10100	1810
278	1480	2820	2570	12700	7080	8370	5310	6050	10000	1810
279	1420	2860	2590	13100	7430	8140	5380	5810	9960	1820
280	1360	2880	2570	13400	7780	7940	5450	5560	9800	1820
281	1330	2870	2520	13700	8110	7750	5550	5320	9620	1810
282	1290	2830	2440	14000	8430	7580	5660	5080	9430	1790
283	1210	2780	2360	14200	8740	7430	5780	4840	9220	1750
284	1080	2710	2290	14400	9030	7310	5870	4610	9010	1700
285	897	2640	2180	14600	9300	7210	5930	4370	8790	1630
286	708	2540	2000	14700	9550	7130	5970	4130	8560	1570
287	526	2410	1750	14800	9780	7070	6020	3900	8340	1520
288	376	2240	1450	14900	9990	7020	6090	3670	8110	1480
289	255	2030	1100	14900	10200	7000	6170	3400	7870	1460
290	170	1800	836	14900	10500	6990	6260	3180	7550	1440
291	112	1580	607	14900	10700	6990	6300	2960	7300	1430
292	71	1370	424	14800	10800	7000	6330	2740	7040	1420
293	45.3	1200	289	14700	11000	7020	6380	2520	6770	1420
294	28	1050	192	14700	11100	7040	6440	2310	6490	1410
295	17.7	924	125	14600	11200	7040	6490	2100	6190	1400
296	11	828	81.5	14500	11200	7050	6540	1900	5890	1400
297	6.7	748	52.5	14500	11300	7040	6570	1700	5570	1400
298	4.0	682	34.1	14500	11300	7020	6640	1500	5230	1400
299	2.5	628	22.1	14500	11400	6980	6690	1320	4900	1390
300	1.5	582	14.4	14600	11400	6920	6730	1210	4560	1380
301	0.93	542	9.3	14700	11500	6840	6770	1050	4200	1370
302	0.56	508	6.1	14800	11500	6750	6810	909	3800	1360
303	0.35	478	3.9	14900	11600	6650	6860	787	3450	1350
304	0.23	452	2.6	15000	11700	6530	6880	677	3120	1330
305	0.14	428	1.7	15100	11800	6370	6900	581	2800	1320
306	0	407	1.3	15200	11900	6210	6910	498	2480	1310
307		387	0.98	15400	12100	6030	6920	426	2180	1300
308		369	0.75	15500	12200	5850	6940	364	1910	1280
309		353	0.57	15600	12300	5670	6960	311	1660	1260
310		338	0.43	15700	12500	5470	6980	264	1430	1240
311		323	0.33	15800	12700	5260	6990	222	1220	1220
312		310	0.25	15800	12900	5040	6970	189	1030	1200

wave length (nm)	TYR	GA	VAL	*trans*-FA		*cis*-FA		SyrAcid		SA
				pH 5	pH 2	pH 5	pH 2	pH 5	pH 2	
313		297	0.19	15800	13100	4800	6920	156	889	1170
314		284	0.15	15800	13300	4550	6880	127	739	1140
315		273	0.11	15700	13500	4310	6840	104	610	1110
316		263	0	15700	13600	4080	6790	81.8	496	1080
317		252		15500	13800	3850	6760	66.1	401	1060
318		242		15400	13900	3620	6700	52.8	323	1020
319		232		15100	14000	3440	6610	41.7	257	994
320		222		14900	14100	3270	6530	33.3	204	962
321		213		14600	14200	3110	6480	26.6	161	928
322		204		14300	14200	2970	6410	21.2	126	892
323		195		13800	14200	2850	6300	16.8	97.9	856
324		186		13400	14100	2740	6180	14.1	76.5	824
325		178		13000	14100	2640	6080	11.7	60.0	792
326		169		12500	13900	2570	5970	9.8	46.5	756
327		161		12000	13800	2500	5830	8.2	35.9	710
328		152		11500	13600	2430	5720	6.8	27.5	674
329		144		10900	13400	2370	5570	5.7	21.2	642
330		136		10400	13200	2290	5400	4.6	16.5	598
331		127		9770	12900	2220	5240	3.8	12.6	558
332		119		9180	12500	2150	5070	3.0	9.7	524
333		111		8610	12200	2100	4920	2.6	7.5	494
334		103		8050	11800	2070	4740	2.4	5.8	458
335		96		7500	11400	2030	4570	1.9	4.4	422
336		89.3		6950	11000	2000	4370	1.7	3.6	390
337		82.8		6410	10500	1940	4150	1.4	3.1	362
338		76.7		5910	9940	1890	3920	0.99	2.6	336
339		70.9		5440	9460	1810	3730	0.81	2.0	306
340		65.5		5000	8970	1730	3470	0.68	1.7	284
341		60.8		4610	8490	1640	3320	0.64	1.6	260
342		56.6		4240	8010	1570	3160	0.62	1.4	240
343		53.1		3890	7560	1490	3000	0.75	1.3	218
344		49.5		3560	7120	1420	2830	0.61	0	204
345		46.4		3270	6680	1340	2670	0.29		188
346		43.5		3000	6260	1260	2520	0.27		168
347		40.8		2740	5830	1190	2390	0.17		158
348		38.5		2510	5420	1150	2260	0		152
349		36.4		2290	4920	1100	2120			148
350		34.5		2090	4550	1050	1990			144
351		32.6		1890	4180	974	1860			138
352		30.8		1710	3810	898	1720			126
353		29.3		1530	3480	828	1590			118

wave length (nm)	TYR	GA	VAL	*trans*-FA		*cis*-FA		SyrAcid		SA
				pH 5	pH 2	pH 5	pH 2	pH 5	pH 2	
354		28.0		1380	3150	760	1470			122
355		26.5		1230	2850	692	1360			116
356		24.9		1100	2570	627	1250			108
357		23.6		977	2300	568	1150			106
358		22.4		870	2060	515	1050			96
359		21.4		771	1830	467	960			86
360		20.2		682	1630	424	873			88
361		19.2		602	1450	381	789			84
362		18.8		533	1290	342	719			72
363		18.1		471	1150	306	657			68
364		17.1		417	1010	275	601			74
365		16.4		366	896	246	545			70
366		15.8		322	788	221	489			68
367		15.0		281	690	196	437			72
368		14.2		244	601	173	388			72
369		13.4		212	523	153	350			70
370		12.7		184	454	135	316			66
371		12.4		159	393	118	281			62
372		11.9		137	337	103	248			60
373		11.3		118	290	90.7	218			60
374		10.6		101	250	79.6	193			56
375		10.1		86.6	213	69.2	171			52
376		9.6		73.8	181	60.3	153			54
377		9.1		63.1	154	52.3	135			54
378		8.7		54.2	131	45.3	119			44
379		8.5		46.8	113	39.7	105			44
380		8.2		40.3	97	34.7	92			46
381		7.7		34.4	83	30.1	80			46
382		7.3		29.5	71	26.3	69			38
383		7.0		25.6	60	22.5	62			34
384		6.7		22	51	19.1	55			40
385		6.5		19	43	16.7	51			40
386		6.3		16.2	37	14.8	44			38
387		5.9		13.4	31	12.3	37			34
388		5.7		11	26	10.6	33			26
389		5.4		9.3	22	8.4	28			30
390		5.1		8.0	18	6.7	22			28
391		5.0		0	0	0	0			22
392		4.9								20
393		4.6								18
394		4.2								20

wave length (nm)	TYR	GA	VAL	*trans*-FA		*cis*-FA		SyrAcid		SA
				pH 5	pH 2	pH 5	pH 2	pH 5	pH 2	
395		3.9								18
396		3.9								16
397		3.8								12
398		3.6								12
399		3.3								14
400		3.1								12
401		3.1								0
402		3.0								
403		2.9								
404		2.8								
405		2.7								
406		2.6								
407		2.5								
408		2.4								
409		2.2								
410		2.0								
411		2.0								
412		2.0								
413		1.8								
414		1.7								
415		1.7								
416		1.7								
417		1.7								
418		1.6								
419		1.5								
420		1.5								
421		1.5								
422		1.4								
423		1.2								
424		1.2								
425		1.2								
426		1.2								
427		1.1								
428		1.1								
429		1.0								
430		1.0								
431		0.96								
432		0.80								
433		0.69								
434		0.67								
435		0.70								
436		0.69								

wave length (nm)	TYR	GA	VAL	*trans*-FA		*cis*-FA		SyrAcid		SA
				pH 5	pH 2	pH 5	pH 2	pH 5	pH 2	
437		0.61								
438		0.60								
439		0.70								
440		0.75								
441		0.70								
442		0.52								
443		0.49								
444		0.53								
445		0.44								
446		0.37								
447		0.41								
448		0.36								
449		0.32								
450		0.26								
451		0.26								
452		0.28								
453		0.26								
454		0.26								
455		0.20								
456		0.06								
457		0.04								
458		0.10								
459		0.11								
460		0.08								
461		0.04								
462		0								

[a] Ferulic acid has a carboxylic acid group with a pK_a of 4.6 (Erdemgil et al., 2007). Molar absorption coefficients of *trans*- and *cis*-ferulic acid were determined by first measuring the *trans* isomer. As noted above, we prepared five different solutions of *trans*-ferulic acid, which is the isomer received from the vendor. We measured the absorbance of these initial solutions and determined the molar absorptivity directly for *trans*-FA. Next, we illuminated each of the five solutions individually for 20 mins to equilibrate the photoisomerization of FA. We quantified the fraction of each isomer using HPLC and measured the absorbance of the solution after illumination. Then, we determined the molar absorption coefficients of *cis*-FA by $\varepsilon_{\mathrm{cis-FA}} = \frac{Abs_{\mathrm{corrected}}}{l \times [\mathrm{cis-FA}]}$, where $Abs_{\mathrm{corrected}}$ is the absorbance of the solution corrected to remove the absorbance contribution from *trans*-FA, l is the cell path length (1 cm), and [cis-FA] is the concentration of the cis-isomer in M, as determined by HPLC.

[b] Syringic acid has a carboxylic group with a pK_a of 4.2 (Erdemgil et al., 2007).

Table S3. ArOH Decay Kinetics by •OH[a]

Phenol	k'_{light} [b] (10^{-4} s^{-1})	j_{ArOH} [c] (10^{-4} s^{-1})	k'_{ArOH} [d] (10^{-4} s^{-1})	$[•OH]_{exp}$ [e] (10^{-15} M)
TYR	0.89	≈ 0	1.3	8.9
GA	0.88	≈ 0	1.2	8.2
VAL	0.96	≈ 0	1.3	8.4
FA [f]	0.91	0.041	1.2	6.5
SyrAcid	2.9	0.45	3.6	18
SA	3.4	0.65	4.1	17

[a] Concentrations of reactants are in Table S1. The photolysis rate constant for 2-nitrobenzaldehyde, our chemical actinometer, was measured once during our •OH experiments, with a value of 5.0×10^3 s^{-1}.

[b] Experimentally determined pseudo-first-order rate constant for the decay of ArOH by •OH, determined as the negative of the slope of $\ln([ArOH]/[ArOH]_0)$ versus reaction time (Figure S2).

[c] Previously measured photolysis rate constants under midday, Davis winter-solstice sunlight for ArOH in simulated sunlight from Arciva et al. (2022).

[d] Corrected pseudo-first-order decay constant for ArOH loss by •OH, determined by $k'_{\mathrm{ArOH}} = \left[\left(\frac{k'_{\mathrm{light}}}{j_{\mathrm{2NB}}}\right) \times j_{\mathrm{2NB,win}}\right] - j_{\mathrm{ArOH}}$. We normalized values to sunlight conditions at midday on the winter solstice at Davis ($j_{2NB,win} = 0.0070$ s^{-1}) (Anastasio and McGregor, 2001).

[e] Steady-state concentrations of •OH in experimental solutions (normalized to winter-solstice sunlight) estimated by $[•OH] = \frac{k'_{\mathrm{ArOH}}}{k_{\mathrm{ArOH+OH}}}$, where $k_{ArOH+OH}$ (M^{-1} s^{-1}) is the second-order rate constant of ArOH with •OH (Arciva et al., 2022).

[f] Values for FA represent a weighted average between the *cis* and *trans* isomers.

Table S4. ArOH Decay Kinetics by $^3C^*$

Phenol	j_{2NB} [a] (10^{-4} s^{-1})	k'_{light} [b] (10^{-4} s^{-1})	k'_{ArOH} [c] (10^{-4} s^{-1})	$[^3C^*]_{exp}$ [d] (10^{-14} M)
TYR	59	0.16	0.19	4.0
GA	65	0.50	0.54	2.9
VAL	100	0.31	0.21	1.2
FA [e]	61	0.37	0.38	4.6
SyrAcid	61	2.4	2.4	11
SA	61	2.6	2.4	8.7

[a] Photolysis rate constant for 2-nitrobenzaldehyde, a chemical actinometer, on the day of an aqSOA experiment.

[b] Pseudo-first-order rate constant for the decay of ArOH by oxidizing triplets, determined from the slope of the plot ln([ArOH]/[ArOH]$_0$) versus reaction time (Figure S2).

[c] Corrected pseudo-first-order decay of ArOH by $^3C^*$, determined by $k'_{ArOH} = \left[\left(\frac{k'_{light}}{j_{2NB}}\right) \times j_{2NB,win}\right] - j_{ArOH}$. Values of j_{ArOH}, the direct photodegradation rate constant for each phenol normalized to Davis winter-solstice sunlight, are in Table S2. k'_{ArOH} values are normalized to sunlight conditions at midday on the winter solstice at Davis ($j_{2NB,win}$ = 0.0070 s^{-1}) (Anastasio and McGregor, 2001).

[d] Steady-state concentration of $^3C^*$ in experimental solutions (normalized to winter-solstice sunlight) estimated by $[^3C^*] = \frac{k'_{ArOH}}{k_{ArOH+3C^*}}$, where $k_{ArOH+3C^*}$ (M^{-1} s^{-1}) as the second-order rate constant of ArOH with $^3C^*$ (Ma et al., 2021).

[e] Values for FA represent a weighted average between the *cis* and *trans* isomers.

Table S5. aqSOA Mass Yields for highly substituted ArOH

Compound	$^{\bullet}$OH Reaction aqSOA Mass Yield (± 1σ)[a]	^{3}C* Reaction aqSOA Mass Yield (± 1σ)[b]
TYR	94.3 (± 3.6)	85.9 (± 3.9)
GA	65.5 (± 7.8)	84.5 (± 3.8)
VAL	73.7 (± 3.1)	59.0 (± 2.0)
FA	83.1 (± 6.1)	90.6 (± 13.8)
SyrAcid	63.8 (± 2.7)	78.5 (± 8.6)
SA	81.4 (± 4.9)	99.1 (± 7.9)
Avg (± 1σ)	82 (± 12)	83 (± 14)

[a] AqSOA mass yields are an average of measurements of samples at one, two, and three half-lives (i.e., $t_{1/2}$, $2t_{1/2}$, $3t_{1/2}$) (Arciva et al., 2022).

[b] AqSOA mass yields are an average of measurements of samples at one, two, and three half-lives (i.e., $t_{1/2}$, $2t_{1/2}$, $3t_{1/2}$) (Ma et al., 2021).

Table S6. MAC_{ArOH} and $MAC_{aqSOA,t1}$ for ArOH reacting with $^{\bullet}OH$ or $^{3}C^{*}$. MAC values (in units of $m^2\ g^{-1}$) at 300 nm for the parent ArOH (MAC_{ArOH}) and for the aqSOA at the first sampled time point ($MAC_{aqSOA,t1}$) with reaction time as marked. For aqSOA values, we subtracted the absorbance contribution from the reactants (i.e., unreacted ArOH and oxidant precursor).

		$^{\bullet}OH$ Reaction	$^{3}C^{*}$ Reaction
Phenol	MAC_{ArOH}	$MAC_{aqSOA,t1}$	$MAC_{aqSOA,t1}$
TYR	0.00	0.63 (110 min)	1.7 (150 min)
GA	0.88	3.0 (70 min)	3.3 (90 min)
VAL	0.02	3.4 (60 min)	3.2 (90 min)
FA	9.0	4.4 (60 min)	5.5 (120 min)
SyrAcid	1.5	6.1 (20 min)	9.0 (24 min)
SA	1.7	5.1 (20 min)	6.0 (27 min)

Table S7. Light absorption characteristics of the aqSOA: Fraction of light absorption (R_{abs}) due to short wavelengths, $AAE_{300\text{-}400nm}$, and $\log_{10}(MAC_{405})$. Values are listed as a time series from top to bottom (with times shown in Table S1). R_{abs} data are shown in Figures 4 and S8.

	$^{\bullet}$OH Reactions			^{3}C* Reactions		
Phenol	Fraction of $R_{abs,t1}$ from wavelengths < 400 nm [a]	$AAE_{300\text{-}400nm}$ [b]	$\log_{10}(MAC_{405})$	Fraction of $R_{abs,t1}$ from wavelengths < 400 nm [a]	$AAE_{300\text{-}400nm}$ [b]	$\log_{10}(MAC_{405})$
TYR	0.23	8.8	-1.36	0.38	10.22	-1.05
	0.32	8.8	-1.25	0.37	8.43	-0.80
	0.40	8.7	-1.18	0.45	8.57	-0.83
	0.47	8.6	-1.17	0.39	7.53	-0.67
	0.48	8.6	-1.15	0.46	7.94	-0.76
	0.52	8.6	-1.16	0.53	7.63	-0.73
GA	0.48	9.1	-0.72	0.83	9.6	-0.77
	0.54	9.0	-0.79	0.78	8.7	-0.69
	0.54	8.9	-0.84	0.77	8.4	-0.69
	0.57	9.2	-0.93	0.76	8.3	-0.70
	0.59	9.3	-0.98	0.77	8.3	-0.72
	0.59	9.3	-1.04	0.77	8.3	-0.74
VAL	0.25	10.1	-0.76	0.16	7.5	-0.46
	0.37	9.5	-0.76	0.21	7.5	-0.46
	0.44	9.2	-0.78	0.31	7.2	-0.42
	0.49	9.1	-0.83	0.37	6.8	-0.36
	0.51	8.9	-0.89	0.41	6.8	-0.35
	0.54	8.9	-0.95	0.44	6.8	-0.36
FA	0.67	11	-0.75	0.74	12	-0.83
	0.68	11	-0.79	0.68	11	-0.72
	0.67	10	-0.80	0.71	11	-0.78
	0.68	10	-0.85	0.76	11	-0.84
	0.67	9.9	-0.90	0.71	10	-0.78
	0.68	9.6	-0.93			
SA	0.63	5.0	0.06	0.64	3.7	0.28
	0.67	5.2	-0.01	0.65	3.9	0.26
	0.67	5.3	-0.05	0.65	3.9	0.24
	0.66	5.3	-0.08	0.64	4.0	0.21
	0.67	5.6	-0.14	0.64	4.1	0.18
	0.67	5.7	-0.19	0.64	4.1	0.16
SyrAcid	0.70	15	-1.19	0.55	12	-0.54
	0.48	14	-1.02	0.53	11	-0.51
	0.45	14	-1.07	0.52	11	-0.54
	0.44	14	-1.10	0.49	11	-0.55
	0.41	13	-1.17	0.50	11	-0.58
	0.43	13	-1.31	0.50	11	-0.66

[a] Fraction of the rate of sunlight absorption by aqSOA at the first illumination time point that is due to wavelengths below 400 nm.

[b] Absorption Ångström exponent calculated using $AAE_{300-400nm} = -\frac{ln\frac{MAC_{300}}{MAC_{400}}}{ln\frac{300}{400}}$.

Table S8. Experimental and normalized k'_{Rabs} values.

	•OH Reactions		^{3}C* Reactions	
Phenol	$k'_{Rabs,exp}$[a] (10^{-3} min^{-1})	k'_{Rabs}[b] (10^{-3} min^{-1})	$k'_{Rabs,exp}$[c] (10^{-3} min^{-1})	k'_{Rabs}[d] (10^{-3} min^{-1})
TYR	0.74	1.0	0.080	0.095
GA	2.6	3.6	0.46	0.50
VAL	3.1	4.3	0.24	0.17
FA	1.7	2.4	0.0046	0.0053
SyrAcid	6.7	9.4	3.4	3.9
SA	4.9	6.9	2.4	2.8

[a] Experimentally measured rate constant for loss of the rate of light absorption by •OH-derived aqSOA in the presence of •OH.

[b] Corrected pseudo-first-order decay constant for the loss of light absorption by aqSOA in the presence of •OH determined by $k'_{\mathrm{Rabs}} = \left[\left(\frac{k'_{\mathrm{Rabs,exp}}}{j_{\mathrm{2NB}}}\right) \times j_{\mathrm{2NB,win}}\right]$. We normalized values to sunlight conditions at midday on the winter solstice at Davis ($j_{2NB,win}$ = 0.0070 s^{-1}) (Anastasio and McGregor, 2001).

[c] Experimentally measured rate constant for loss of the rate of light absorption by ^{3}C*-derived aqSOA in the presence of ^{3}C*.

[d] Corrected pseudo-first-order decay constant for the loss of light absorption by aqSOA in the presence of ^{3}C*, determined by $k'_{\mathrm{Rabs}} = \left[\left(\frac{k'_{\mathrm{Rabs,exp}}}{j_{\mathrm{2NB}}}\right) \times j_{\mathrm{2NB,win}}\right]$. We normalized values to sunlight conditions at midday on the winter solstice at Davis ($j_{2NB,win}$ = 0.0070 s^{-1}) (Anastasio and McGregor, 2001).

Table S9. $^{\bullet}OH$ concentrations and rate constants for loss of absorbance under experimental solutions and extrapolated to ambient conditions in aerosol liquid water (ALW) and cloud/fog drops (drop).

Phenol	$[^{\bullet}OH]_{exp}$[a] (10^{-15} M)	k'_{Rabs}[b] (10^{-3} min^{-1})	$[^{\bullet}OH]_{drop}$ / $[^{\bullet}OH]_{exp}$[c] (M / M)	$k'_{Rabs,drop}$[d] (10^{-3} min^{-1})	$[^{\bullet}OH]_{ALW}$ / $[^{\bullet}OH]_{exp}$[e] (M / M)	$k'_{Rabs,ALW}$[f] (10^{-3} min^{-1})
TYR	8.9	1.0	0.85	0.88	0.77	0.79
GA	8.2	3.6	0.92	3.4	0.83	3.0
VAL	8.4	4.3	0.91	4.0	0.82	3.5
FA	6.5	2.4	1.2	2.8	1.0	2.5
SyrAcid	18	9.4	0.42	3.9	0.38	3.5
SA	17	6.9	0.46	3.2	0.41	2.9

[a] $^{\bullet}OH$ concentration calculated from the pseudo-first-order loss of ArOH for each experiment (Table S3). Values are normalized to Davis winter-solstice conditions and corrected for j_{ArOH}.

[b] Experimentally determined rate constant for decay of the rate of light absorption by aqSOA determined by the plot of the natural log of the total rate of light absorption from 280 to 800 nm (Equation 1) versus reaction time.

[c] Ratio of $[^{\bullet}OH]$ estimated in fog drops to the $^{\bullet}OH$ concentration in our experiment. Both conditions are normalized to midday winter-solstice sunlight in Davis. For fog drops we use the Ma et al. (2024) estimate of $[^{\bullet}OH]_{drop} = 7.6 \times 10^{-15}$ M for the average of four particle types and a dilution condition typical of a fog drop (3×10^{-5} µg-PM / µg-water).

[d] Estimated rate constant for loss of the rate of light absorption by aqSOA in a fog/cloud drop, determined as the measured (and sunlight-normalized) value of k'_{Rabs} multiplied by the ratio $[^{\bullet}OH]_{drop} / [^{\bullet}OH]_{exp}$.

[e] Ratio of $[^{\bullet}OH]$ estimated in aerosol liquid water to the $^{\bullet}OH$ concentration in our experiment; both values are normalized to winter-solstice sunlight. We use an estimate of $[^{\bullet}OH]_{ALW} = 6.8 \times 10^{-15}$ M for 1 µg-PM / 1 µg-water for the average of four particle types, which were significantly influenced by residential wood combustion, from Ma et al. (2024).

[f] Estimated rate constant for loss of the rate of light absorption by aqSOA in ALW, determined as the measured (and sunlight-normalized) value of k'_{Rabs} multiplied by the ratio $[^{\bullet}OH]_{ALW} / [^{\bullet}OH]_{exp}$.

Table S10. $^3C^*$ concentrations and rate constants for loss of absorbance under experimental solutions and extrapolated to ambient conditions in aerosol liquid water (ALW) and cloud/fog drops (drop).

Phenol	$[^3C^*]_{exp}$[a] (10^{-14} M)	k'_{Rabs}[b] (10^{-3} min^{-1})	$[^3C^*]_{drop}$ / $[^3C^*]_{exp}$[c] (M / M)	$k'_{Rabs,drop}$[d] (10^{-3} min^{-1})	$[^3C^*]_{ALW}$ / $[^3C^*]_{exp}$[e] (M / M)	$k'_{Rabs,ALW}$[f] (10^{-3} min^{-1})
TYR	4.0	0.095	0.89	0.084	14	1.4
GA	2.9	0.50	1.3	0.62	20	10
VAL	1.2	0.17	3.1	0.51	49	8.3
FA	4.6	0.0053	0.77	0.0041	13	0.066
SyrAcid	11	3.9	0.32	1.2	5.2	20
SA	8.7	2.8	0.41	1.1	6.7	18

[a] $^3C^*$ concentration calculated from the pseudo-first-order loss of ArOH for each experiment (Table S4). Values are normalized to Davis winter-solstice conditions and corrected for j_{ArOH}.

[b] Experimentally determined rate constant for decay of the rate of light absorption by aqSOA determined by the plot of the natural log of the total rate of light absorption from 280 to 800 nm (Equation 1) versus reaction time.

[c] Ratio of $[^3C^*]$ estimated in fog drops to the $^{\bullet}OH$ concentration in our experiments. Both values are normalized to winter-solstice sunlight. For fog drops we use the Ma et al. (2024) estimate of $[^3C^*]_{drop} = 3.6 \times 10^{-14}$ M for the average of four particle types and a dilution condition typical of fog drops (3×10^{-5} µg-PM / µg-water).

[d] Estimated rate constant for loss of the rate of light absorption by aqSOA in a fog/cloud drop, determined as the measured (and sunlight-normalized) value of k'_{Rabs} multiplied by the ratio $[^3C^*]_{drop} / [^3C^*]_{exp}$.

[e] Ratio of $[^3C^*]$ estimated in aerosol liquid water to the $^3C^*$ concentration in our experiment; both values are normalized to winter-solstice sunlight. We use an estimate of $[^3C^*]_{ALW} = 5.8 \times 10^{-13}$ M for 1 µg-PM / 1 µg-water for the average of four particle types, which were significantly influenced by residential wood combustion, from Ma et al. (2024).

[f] Estimated rate constant for loss of the rate of light absorption by aqSOA in ALW, determined as the measured (and sunlight-normalized) value of k'_{Rabs} multiplied by the ratio $[^3C^*]_{ALW} / [^3C^*]_{exp}$.

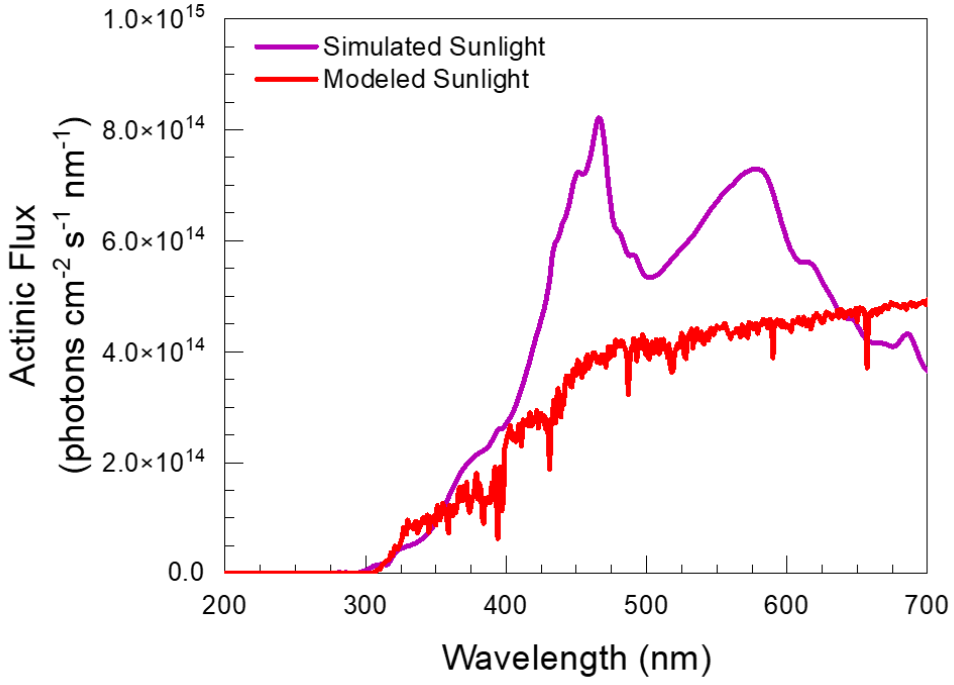

Figure S1. Experimental and simulated actinic flux. The red line is the modeled, midday Davis winter-solstice actinic flux from the Tropospheric Ultraviolet and Visible Radiation Model Version 5.3 (https://www.acom.ucar.edu/Models/TUV/Interactive_TUV/). The purple line is the measured photon flux from our solar simulator on a day with $j_{2NB} = 0.0051$ s^{-1}. The solar simulator contains a 1000 W Xe lamp equipped with a downstream water filter, an AM1.0 air mass filter (AM1D-3L, Sciencetech), and a 295 nm long-pass filter (20CGA-295, Thorlabs).

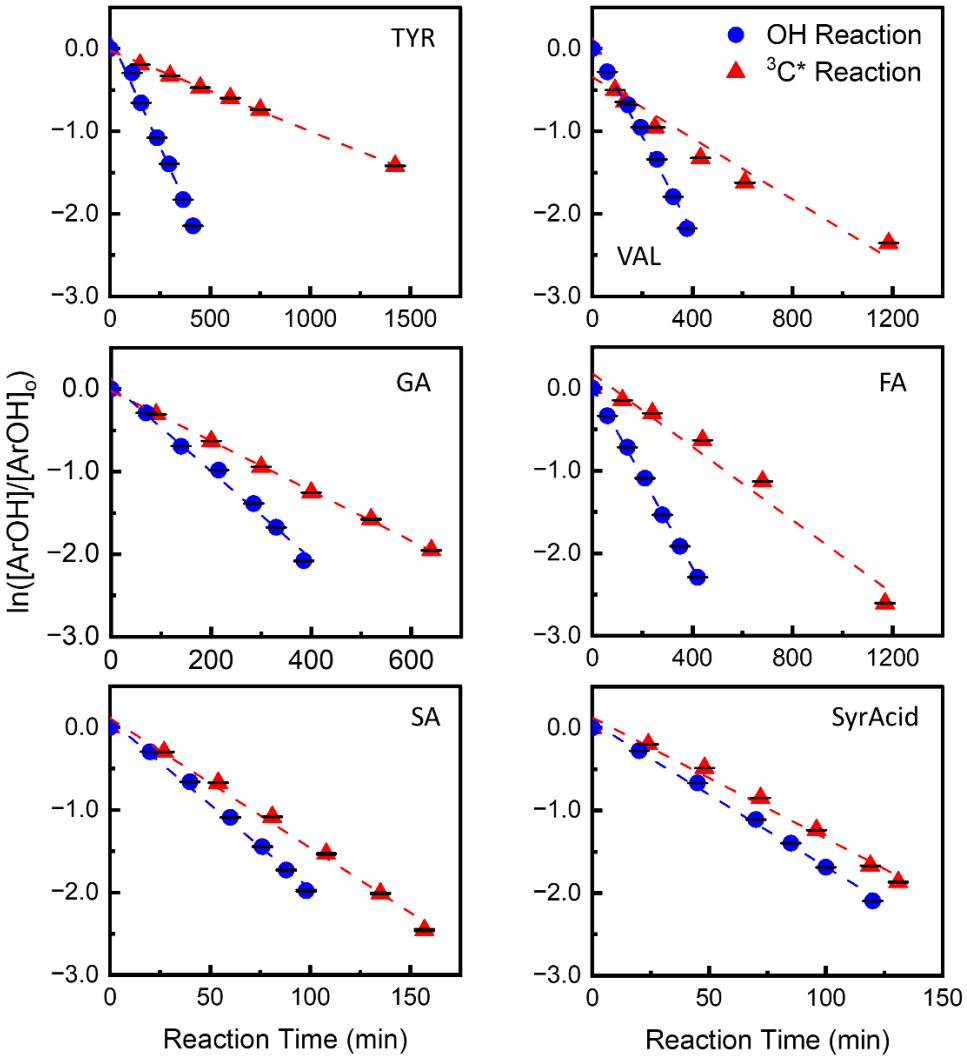

Figure S2. ArOH oxidation kinetics with •OH (blue circles) and $^3C^*$ (red triangles). Error bars represent one standard deviation, determined from the variability in the corresponding dark control.

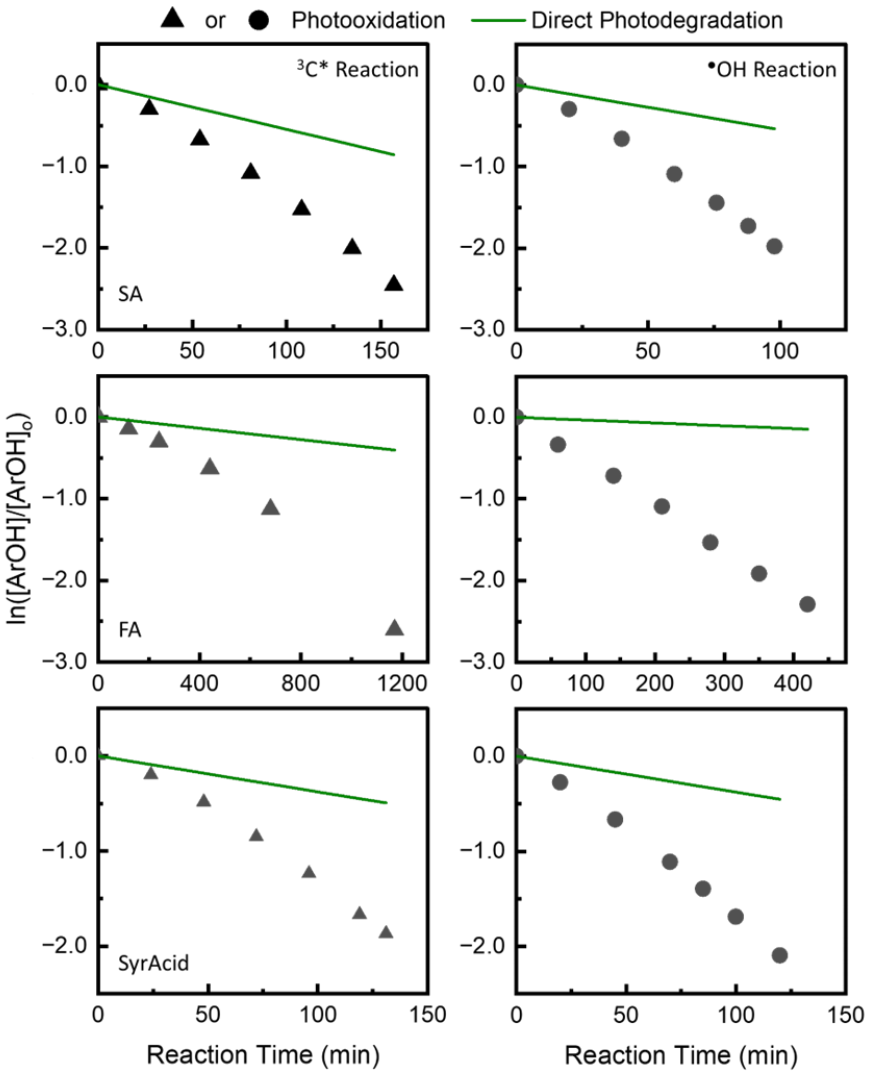

Figure S3. Comparison of direct photodegradation of SA, FA, and SyrAcid (green solid lines), calculated based on rate constants measured in Ma et al. (2021) and normalized to the j_{2NB} of each experiment (Tables S3 and S4) using $j_{ArOH,exp} = \left[\left(\frac{j_{ArOH}}{j_{2NB,WIN}}\right) \times j_{2NB,exp}\right]$, compared to the total photodegradation measured in each experiment (points). Direct photodegradation contributed to 27-35%, 6-15%, and 22-27% to the loss of SA, FA, and SyrAcid, respectively. There was no significant photodegradation for the other three phenols studied.

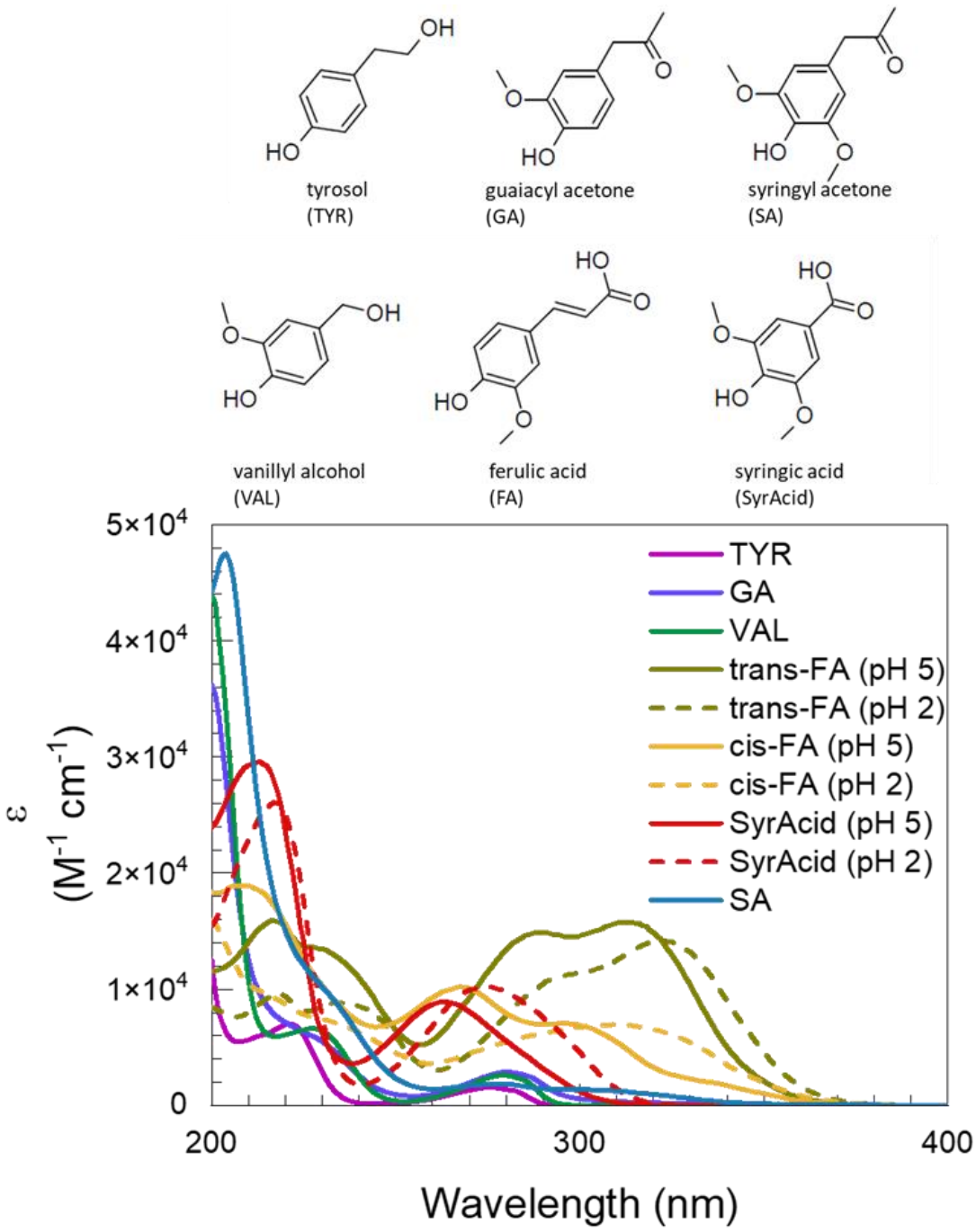

Figure S4. Top: Chemical structures of the six highly substituted ArOH in this study. Bottom: Base-10 molar absorption coefficients (ε) for aqueous, highly substituted ArOH. Values, which are tabulated in Table S2, were determined from the spectra of five different solutions of each ArOH at concentrations of 25, 100, 500, 1000, and 2000 μM in a 1 cm cell.

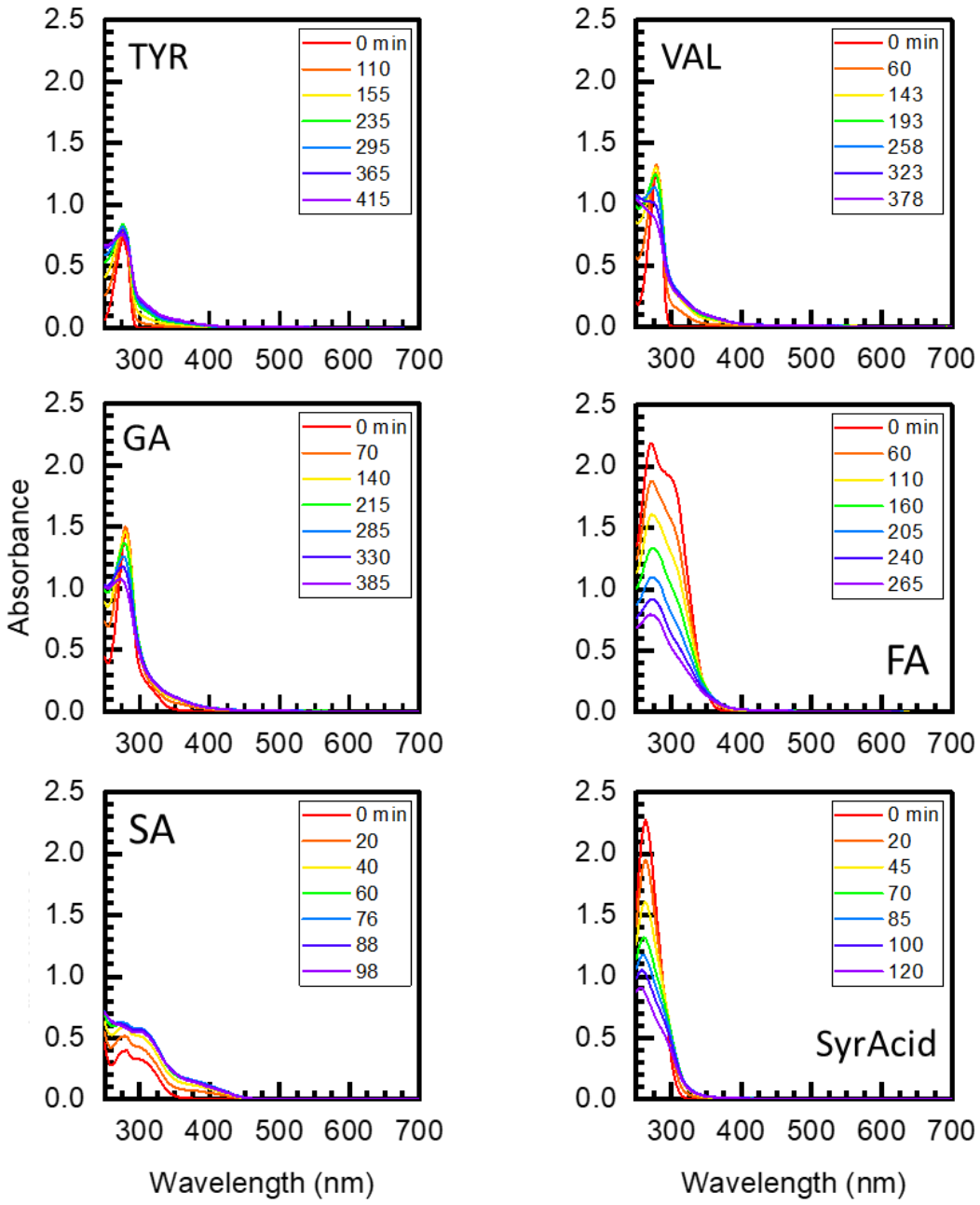

Figure S5. Absorbance measurements for mixtures during the •OH reactions. The absorbance here, which was measured in a 5-cm cell at each time point, represents contributions from the oxidant precursor, starting phenol, and products.

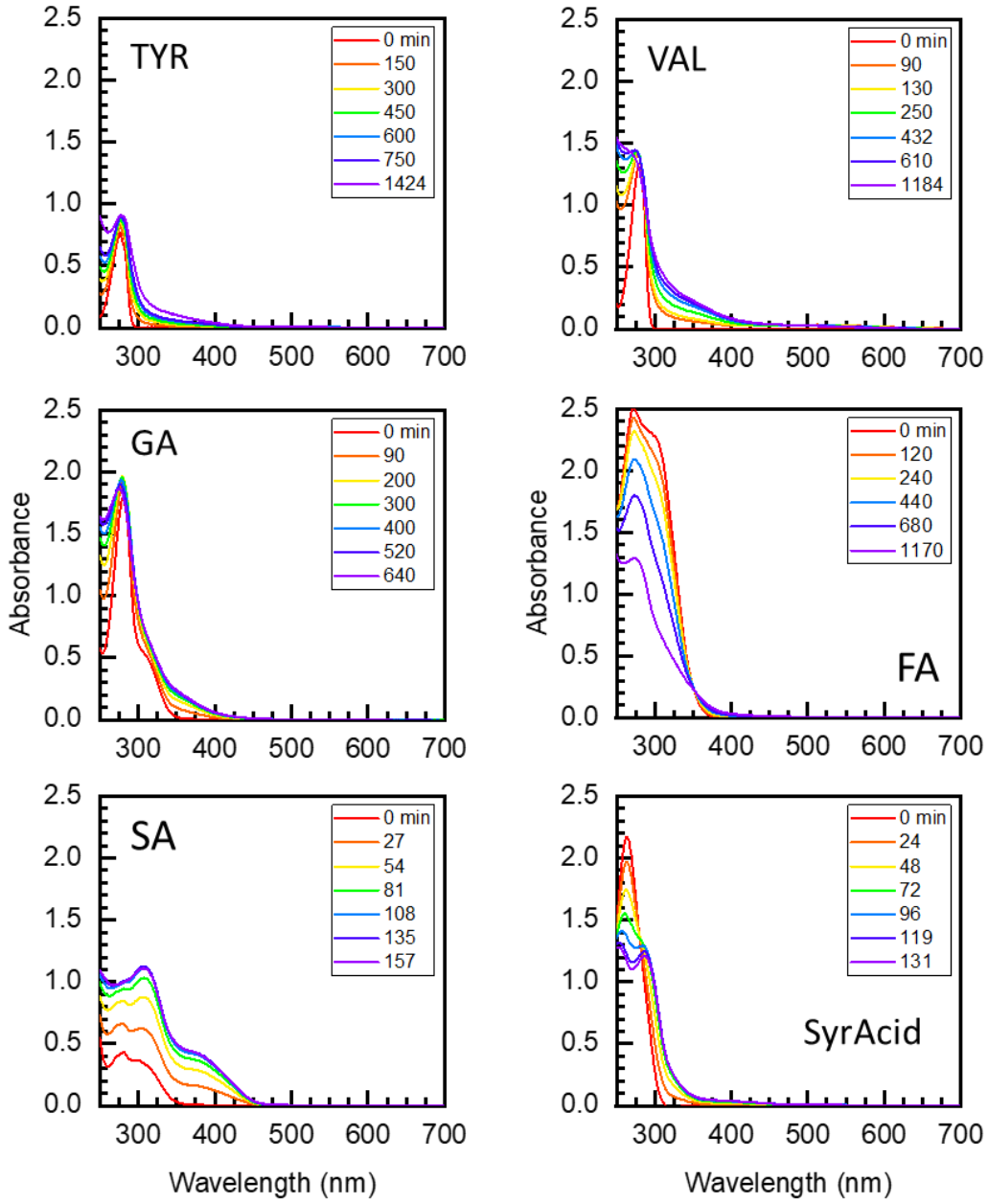

Figure S6. Absorbance measurements for mixtures during $^{3}C^{*}$ reactions. The absorbance here, which was measured in a 5-cm cell at each time point, is due to the oxidant precursor, starting phenol, and products.

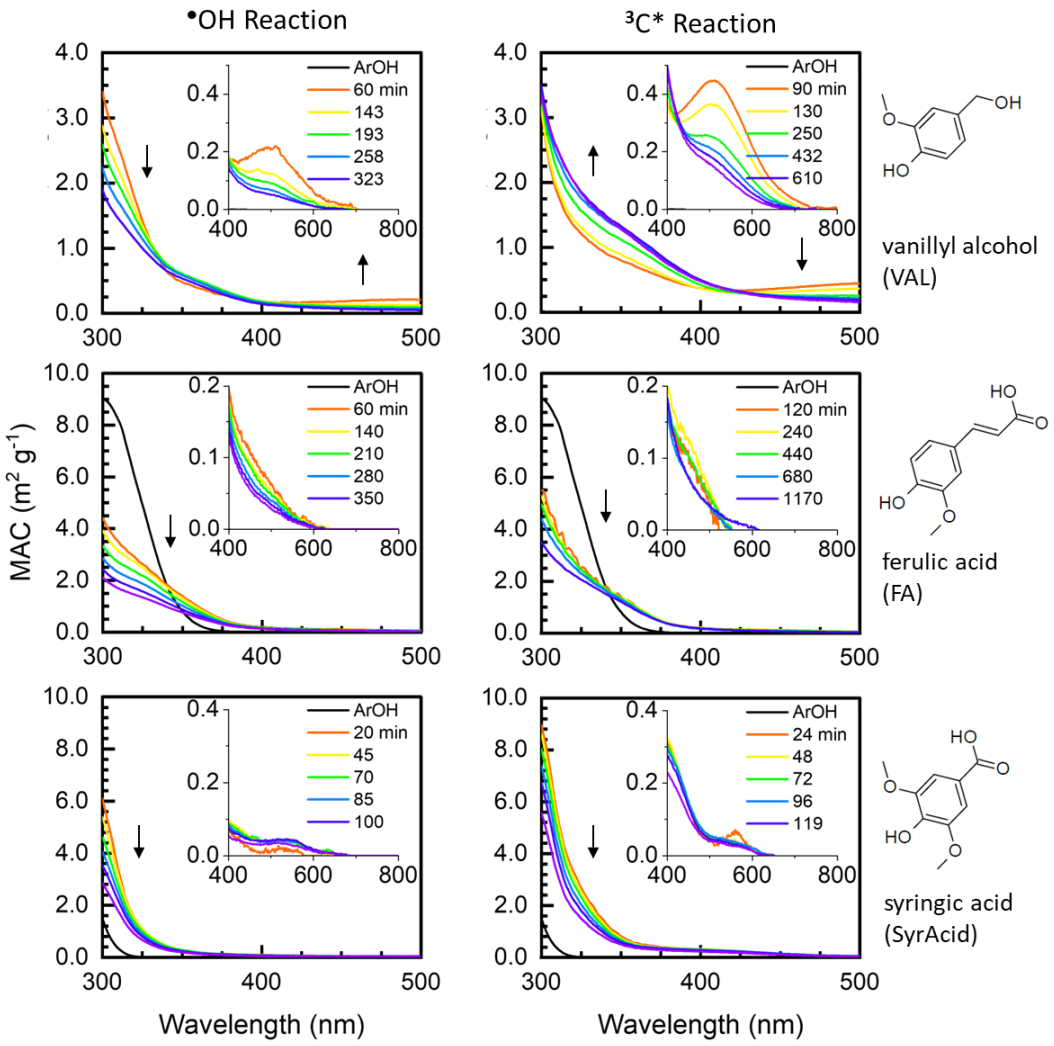

Figure S7. Evolution of mass absorption coefficients (MAC) of aqSOA formed from the •OH reaction (left column) and $^3C^*$ reaction (right column) of three phenols: vanillyl alcohol (top pair of panels), ferulic acid (middle pair), and syringic acid (bottom pair). Arrows show the trend in MAC (i.e., increasing or decreasing) in a given wavelength region as a function of illumination time. The MAC value for each starting phenol is shown as a black line. The absorbance contributions of the starting phenol and oxidant precursor (i.e., H_2O_2 or DMB) have been removed from the aqSOA MAC values (colored lines).

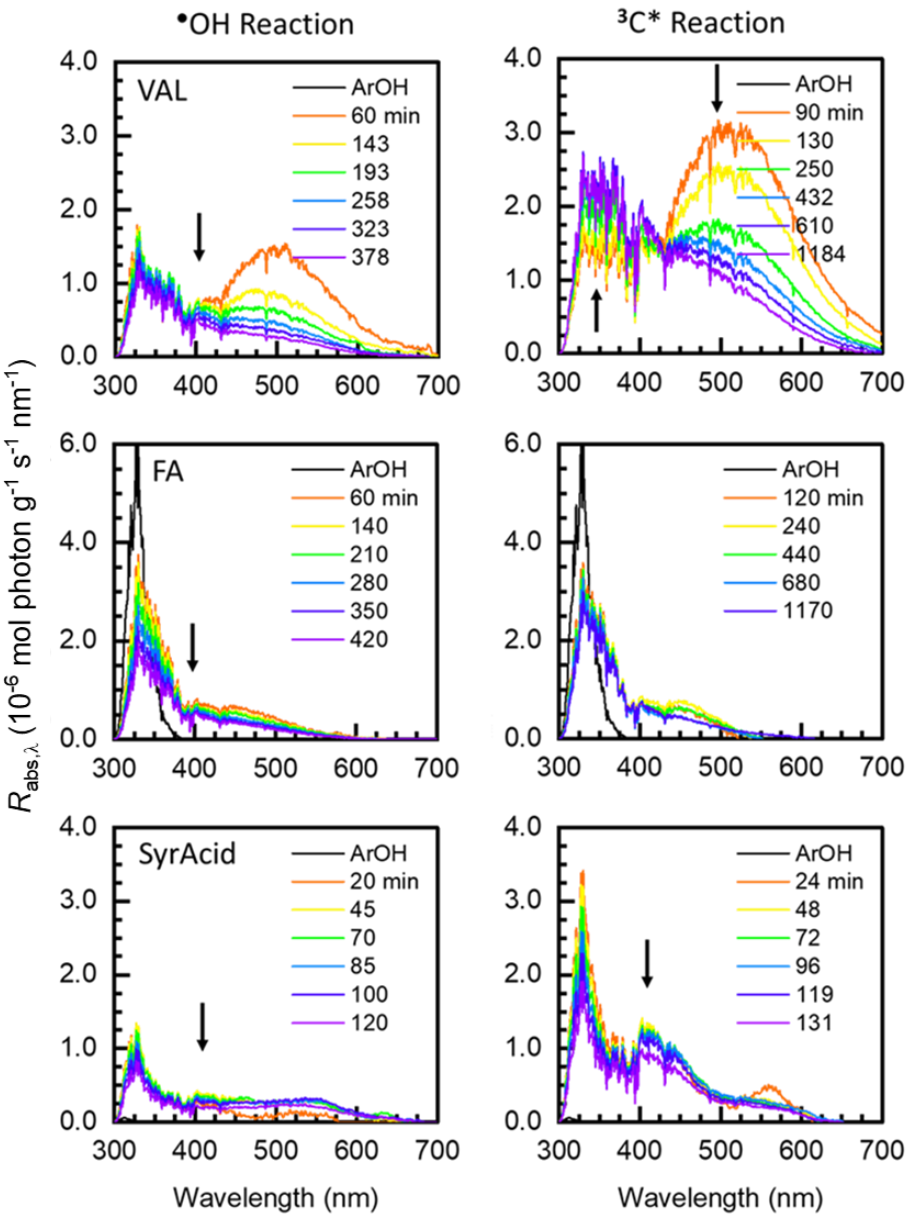

Figure S8. Rates of sunlight absorption for aqSOA formed from vanillyl alcohol (VAL; top), ferulic acid (FA; middle), and syringic acid (SyrAcid; bottom). The left column shows results for reactions of each phenol with •OH while the right column shows the parallel results for ^{3}C* (right column) over the course of illumination. For a given phenol, the black line represents sunlight absorption by the parent ArOH and the colored lines are sunlight absorption for aqSOA at different illumination times. Arrows represent the time trends of aqSOA MAC values after the initial illumination time point.

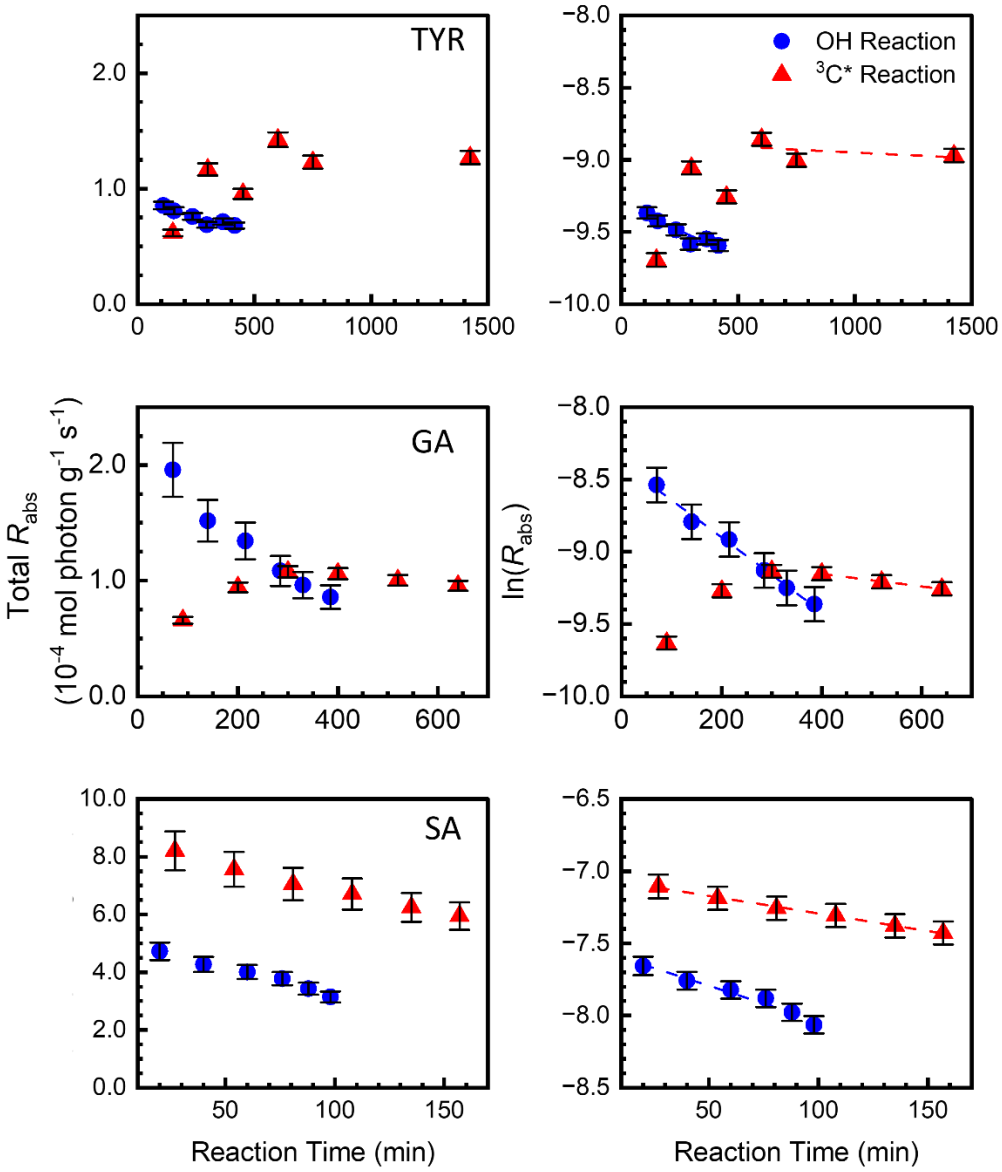

Figure S9. Decay in the rate of sunlight absorption (R_{abs}, 10^{-4} mol photon g^{-1} s^{-1}) for aqSOA formed from tyrosol (TYR), guaiacylacetone (GA), and syringyl acetone (SA) during continued reaction. The left column shows the total rate of aqSOA light absorption (from 280 to 800 nm) over the course of each illumination. The right column shows the same data, but with the natural log of the total rate of light absorption; these plots were used to determine the pseudo-first-order decay of light absorption by aqSOA during illumination. Dashed lines indicate the time points used to determine k'_{Rabs} values (Equation 1) for the reactions with triplets (red triangles and lines) and •OH (blue circles and lines). Error bars represent one standard deviation, determined by propagating the standard deviation in HPLC measurements of ArOH decay with the uncertainty of the aqSOA mass yield measurements.

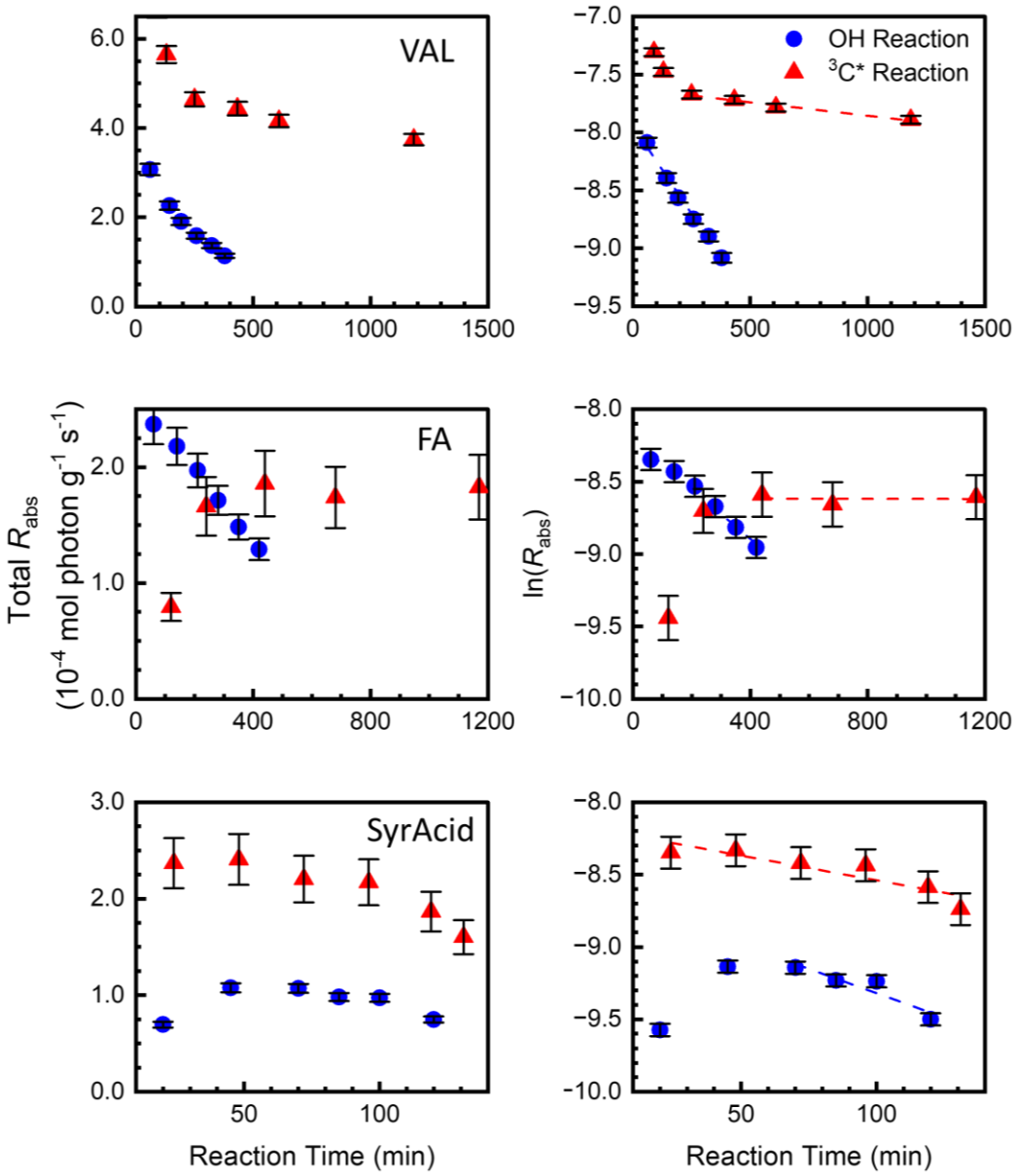

Figure S10. Decay in the rate of sunlight absorption (R_{abs}, 10^{-4} mol photon g^{-1} s^{-1}) for aqSOA formed from vanillyl alcohol (VAL), ferulic acid (FA), and syringic acid (SyrAcid). The left column shows the total rate of aqSOA light absorption (summed from 280 to 800 nm) at each sampled time point. The right column shows the same data, but with the natural log of the total rate of light absorption; these plots were used to determine the pseudo-first-order decay of light absorption by aqSOA during illumination. Dashed lines indicate the time points used to determine k'_{Rabs} values (Equation 1) for the reactions with triplets (red) and •OH (blue). Error bars represent one standard deviation, determined by propagating the standard deviation in HPLC measurements of ArOH decay with the uncertainty of the aqSOA mass yield measurements.

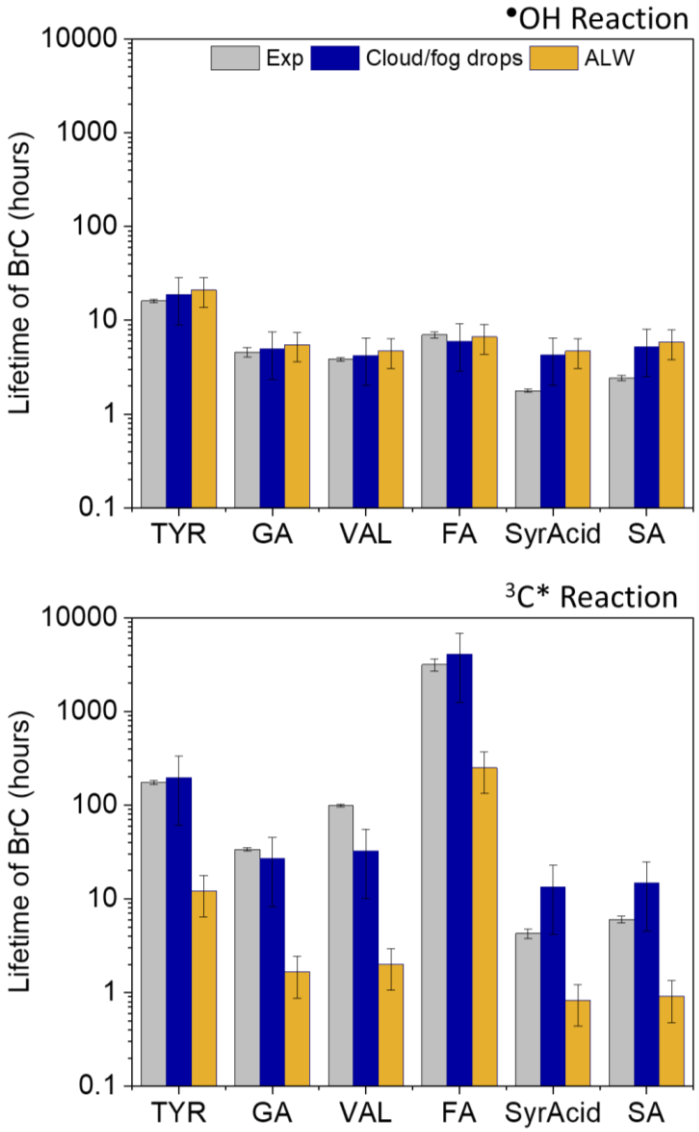

Figure S11. Lifetimes of phenolic BrC formed from •OH and ^{3}C* reactions. Top panel: Lifetimes of •OH-formed BrC with respect to •OH oxidation under conditions of: (a) our experiments (gray bars), (b) cloud/fog drops (blue bars), and (c) ALW (gold bars). Bottom panel: Lifetime of light absorption by triplet-formed BrC with respect to oxidation by triplets. Error bars for experimental conditions represent one standard deviation determined from the relative standard deviation in the rate of aqSOA light absorption. Errors for ALW and cloud/fog drop conditions were calculated using the RSD of the rate of aqSOA light absorption propagated with the relative standard deviation of the photooxidant concentration measurements and predictions in Ma et al. (2024).

Section S1. Potential Contributions of $^{\bullet}OH$ and $^1O_2$* in ^{3}C* Experiments

In this section we assess the potential contributions of two secondary oxidants - $^{\bullet}OH$ and singlet molecular oxygen ($^1O_2$*) - towards phenol loss in our triplet experiments. Hydroxyl radical will be formed because reactions of triplet excited states with phenols form hydrogen peroxide (H_2O_2) (Anastasio et al., 1997), which undergoes direct photolysis to make $^{\bullet}OH$. In addition, the reaction of a triplet excited state with dissolved oxygen forms $^1O_2$* (Zepp et al., 1977). Both $^{\bullet}OH$ and $^1O_2$* can react with aqueous phenols.

To understand the potential significance of ArOH loss by $^{\bullet}OH$, we first calculate the photolysis rate of H_2O_2 (j_{H2O2}, s^{-1}) under our experimental conditions based on results from the $^{\bullet}OH$ experiments:

$$j_{H2O2} = \frac{[OH] \times k'_{sink,OH}}{[H2O2]}, \quad \text{(S1)}$$

where [$^{\bullet}OH$] is the steady-state concentration (Table S3), $k'_{sink,OH}$ is the calculated pseudo-first-order rate constant for the loss of $^{\bullet}OH$ in the $^{\bullet}OH$ experiments (i.e., due to reactions with 2-propanol and ArOH), and [H_2O_2] is the initial molar concentration of hydrogen peroxide in the $^{\bullet}OH$ experiment. Values of j_{H2O2} range from 2.4×10^{-6} to 6.7×10^{-6} s^{-1} in our $^{\bullet}OH$ experiments.

Next, we estimate the concentration of [$^{\bullet}OH$] in the ^{3}C* experiments by:

$$[OH] = \frac{j_{H2O2} \times [H2O2]}{k'_{sink,3C*}}, \quad \text{(S2)}$$

where [H_2O_2] is the estimated concentration at the midway illumination time in the triplet experiment and $k'_{sink,3C*}$ is the calculated pseudo-first-order rate constant for the loss of $^{\bullet}OH$ in the ^{3}C* experiments. Since we did not add 2-PrOH in the ^{3}C* experiments, the $^{\bullet}OH$ sink here is only from the phenol. We ignored the DMB sink for $^{\bullet}OH$ because it is small compared to the phenol sink. To estimate the H_2O_2 concentration in the ^{3}C* experiments, we used the ratio of the quantum yield of H_2O_2 formation to the quantum yield of ArOH loss (0.18) determined from ^{3}DMB* with phenol (Anastasio et al., 1997):

$$\frac{\Delta n_{H2O2}}{\Delta n_{ArOH}} = 0.18. \quad \text{(S3)}$$

That is, 0.18 moles of H_2O_2 are formed for every mole of phenol reacted. We then multiply this ratio by the reduction in the molar concentration of ArOH by the midpoint of the experimental illumination time to estimate the concentration of H_2O_2 formed by this point. At the halfway point in the triplet-mediated degradation of phenols, approximately 63% of the initial ArOH has reacted, which should result in 12 μM of H_2O_2 for experiments with 100 μM initial ArOH and 6 μM H_2O_2 for experiments that started with 50 μM ArOH.

The resulting estimated concentrations of [$^{\bullet}OH$] in the ^{3}C* experiments are all low, on the order of 10^{-17} M, which is several orders of magnitude lower than the experimental [^{3}C*] (Table S4). The result is that $^{\bullet}OH$ accounts for no more than 1% of ArOH loss in our experiments, i.e., photoformed H_2O_2 does not contribute significantly to ArOH loss or aqSOA formation.

The other secondary photooxidant that might be important in our triplet experiments is singlet molecular oxygen, which is formed by the interaction of triplet states with dissolved oxygen. As described by McNeill and Canonica (2016), the concentration of $^1O_2$* in natural waters is approximately equal to the concentration of triplet excited states. Thus, the importance of singlet oxygen as an oxidant for ArOH in our experiments can be estimated by comparing the rate constants of $^1O_2$* and ^{3}C* with phenols. While rate constants for ^{3}DMB* with phenols at pH 5 are (0.1 - 6) × 10^9 M^{-1} s^{-1} (Ma et al., 2021; Smith et al., 2014), values for singlet molecular oxygen with neutral (i.e., not deprotonated) phenols in water are typically (0.1 – 4) × 10^7 M^{-1} s^{-1} (Wilkinson et al., 1995). Thus, we expect that singlet oxygen is typically responsible for a negligible amount (~ 1%) of the phenol loss in our triplet experiments.

Section S2. Absorbance Correction and MAC_{ArOH} Determination

The experimentally measured absorbance of a reaction mixture at a given wavelength ($Abs_{exp,\lambda}$, e.g., Figures S4 and S5) includes contributions from the starting phenol ($Abs_{ArOH,\lambda}$), H_2O_2 or DMB as the oxidant precursor ($Abs_{Ox,\lambda}$), and the aqSOA that formed ($Abs_{aqSOA,\lambda}$):

$$Abs_{exp,\lambda} = Abs_{ArOH,\lambda} + Abs_{Ox,\lambda} + Abs_{aqSOA,\lambda}. \quad \text{(S4)}$$

To calculate the MAC for the parent ArOH (MAC_{ArOH}) in this mixture, we took the absorbance at time 0 (i.e., where $Abs_{aqSOA,\lambda} = 0$) and subtracted the absorbance contribution from the known concentration of either H_2O_2 (in $^{\bullet}OH$ reactions) or DMB (in $^3C^*$ reactions):

$$Abs_{ArOH,\lambda} = Abs_{exp,\lambda}\ at\ time\ zero - Abs_{Ox,\lambda}, \quad \text{(S5)}$$

$$\text{where } Abs_{Ox,\lambda} = \varepsilon_{Ox,\lambda} \times [Ox] \times l. \quad \text{(S6)}$$

The absorbance of the oxidant precursor at wavelength λ was determined as the product of the base-10 molar absorption coefficient of the precursor ($\varepsilon_{Ox,\lambda}$, M^{-1} cm^{-1}), the oxidant precursor concentration ([Ox], M), and the cell path length (l, cm). Values of the oxidant precursor molar absorption coefficients are from Miller and Kester (1988) for H_2O_2 and from Smith et al. (2014) for DMB.

The remaining absorbance at time 0 represents the absorbance of the starting phenol. Absorbance values for the starting phenol can also be calculated using the molar absorption coefficients from Table S2 and equation S7; this procedure results in the same values.

$$Abs_{ArOH,\lambda} = \varepsilon_{ArOH,\lambda} \times [ArOH] \times l \quad \text{(S7)}$$

This parent phenol absorbance was then used to calculate the corresponding MAC:

$$MAC_{ArOH,\lambda}\ (m^2\ g^{-1}) = \frac{2.303 \times Abs_{ArOH,\lambda} \times 10^3 \times 10^{-4}}{l \times [ArOH]} \quad \text{(S8)}$$

where 2.303 converts the absorbance from base-10 to base-e, l is the path length of our cuvette (5 cm), [ArOH] is starting phenol mass concentration (g L^{-1}), the factor of 10^3 converts from L to cm^3, and the factor of 10^{-4} converts from cm^2 to m^2.

For subsequent time points, we calculated the wavelength-specific absorbance of aqSOA in the reaction mixture by removing the absorbance contributions from both the remaining parent phenol and oxidant precursor:

$$Abs_{aqSOA,\lambda} = Abs_{exp,\lambda} - (Abs_{ArOH,\lambda} + Abs_{Ox,\lambda}) \quad \text{(S9)}$$

The absorbance of the phenol at a given reaction time and wavelength was determined as the product of its concentration (determined by HPLC), the molar absorption coefficient at that wavelength (Table S2), and the cell path length, as shown in equation S7. The absorbance of the oxidant precursor was determined as explained in equation S6. For triplet experiments, the DMB concentration determined in the same HPLC run as the ArOH measurement.

Because we did not measure the H_2O_2 concentration, we estimated [H_2O_2] over the course of illumination by considering the stoichiometries of ArOH and H_2O_2 loss during illumination. The main loss of H_2O_2 is through direct photolysis to form $^{\bullet}OH$ (SR1), while reaction with $^{\bullet}OH$ (SR3) is a minor path. Based on the rate constants for SR2 and SR3 (Arciva et al., 2022; Christensen et al., 1982), we calculated the percent of $^{\bullet}OH$ reacting with ArOH or H_2O_2 in each reaction mixture; e.g., for GA, these are 92% and 8%, respectively. Next, we determined the relationships between the change in the number of moles of H_2O_2 (Δn_{H2O2}), $^{\bullet}OH$ formed ($\Delta n_{^{\bullet}OH}$) and GA (Δn_{GA}) in these reactions.

$H_2O_2 \rightarrow 2\ ^{\bullet}OH$ (SR1)

For this reaction, $\Delta n_{H2O2} = 0.5\Delta n_{^{\bullet}OH}$

$^{\bullet}OH + ArOH \rightarrow$ Products (SR2)

Based on the relative rates of SR2 and SR3 as fates of $^{\bullet}OH$, $\Delta n_{^{\bullet}OH} = \Delta n_{GA}/0.92$.

$^{\bullet}OH + H_2O_2 \rightarrow H_2O + HO_2^{\bullet}$ (SR3)

Since 2 $HO_2^{\bullet}$ combine to form 1 molecule of H_2O_2, we can rewrite SR3 as

$^{\bullet}OH + H_2O_2 \rightarrow H_2O + 0.5\ H_2O_2$ (SR4)

Considering the relative importance of SR2 and SR3 as sinks of $^{\bullet}OH$, we can write the relationship

$\Delta n_{^{\bullet}OH} = (\Delta n_{H2O2}/0.08) \times 2 = \Delta n_{H2O2}/0.04$ for SR3.

We can then sum the stoichiometric losses of H_2O_2 and $^{\bullet}OH$ from these reactions to reveal the relationship between the number of moles of H_2O_2 and GA lost:

Total $\Delta n_{H2O2} = 0.5\Delta n_{^{\bullet}OH} + 0.04\Delta n_{^{\bullet}OH} = 0.54\Delta n_{^{\bullet}OH} = 0.54 \times (\Delta n_{GA}/0.92) = 0.59\ \Delta n_{GA}$.

That is, $\frac{\Delta n_{H2O2}}{\Delta n_{GA}} = 0.59$, (S10)

which indicates that the number of moles of H_2O_2 lost during reaction is 59% of the number of moles of GA lost for our conditions. This example is specific for GA, but we performed parallel calculations for the other five phenols. The percentage for reactions of TYR, GA, and VAL average (±1σ) to 59% (±1.0%), and for FA, SyrAcid, and SA, 76% (±4.0%). These percentages are different across the two sets of ArOH due to the different starting concentrations of precursor ArOH and H_2O_2 (Table S1).

The ratio of the change in the number of moles in the reaction solution is equivalent to the ratio expressed as concentrations. Thus, we can determine $\Delta[H_2O_2]_t$, how much the concentration of H_2O_2 changed between adjacent reaction sampling times, by:

$$\Delta[H_2O_2]_t = \Delta[ArOH]_t \times \frac{\Delta n_{H2O2}}{\Delta n_{ArOH}}, \quad \text{(S11)}$$

where $\frac{\Delta n_{H2O2}}{\Delta n_{ArOH}}$ is 0.59 for GA, $\Delta[\mathrm{ArOH}]_t$ is the change in ArOH concentration between two time points as determined by HPLC, and $\Delta[H_2O_2]_t$ is the change in H_2O_2 concentration in M. For use in equation S6 for the •OH experiments, we determined the concentration of H_2O_2 in the reaction solution at a given time using:

$$[\mathrm{H_2O_2}]_t = [\mathrm{H_2O_2}]_o - \Delta[\mathrm{H_2O_2}]_t \quad \text{(S12)}$$

After all of this work, our calculations indicate that the change in H_2O_2 concentration over the course of illumination was small (< 5%) in our •OH experiments, but we still accounted for it.

References

Anastasio, C. and McGregor, K. G.: Chemistry of fog waters in California's Central Valley: 1. In situ photoformation of hydroxyl radical and singlet molecular oxygen, Atmos. Environ., 35(6), 1079–1089, https://doi.org/10.1016/S1352-2310(00)00281-8, 2001.

Anastasio, C., Faust, B. C. and Rao, C. J.: Aromatic Carbonyl Compounds as Aqueous-Phase Photochemical Sources of Hydrogen Peroxide in Acidic Sulfate Aerosols, Fogs, and Clouds. 1. Non-Phenolic Methoxybenzaldehydes and Methoxyacetophenones with Reductants (Phenols), Environ. Sci. Technol., 31(1), 218–232, https://doi.org/10.1021/es960359g, 1997.

Arciva, S., Niedek, C., Mavis, C., Yoon, M., Sanchez, M. E., Zhang, Q. and Anastasio, C.: Aqueous ·OH oxidation of highly substituted phenols as a source of secondary organic aerosol., Environ. Sci. Technol., 56(14), 9959–9967, https://doi.org/10.1021/acs.est.2c02225, 2022.

Christensen, H., Sehested, K. and Corfitzen, H.: Reactions of hydroxyl radicals with hydrogen peroxide at ambient and elevated temperatures, J. Phys. Chem., 86(9), 1588–1590, https://doi.org/10.1021/j100206a023, 1982.

Erdemgil, F. Z., Sanli, S., Sanli, N., Ozkan, G., Barbosa, J., Guiteras, J. and Beltrán, J. L.: Determination of pK(a) values of some hydroxylated benzoic acids in methanol-water binary mixtures by LC methodology and potentiometry., Talanta, 72(2), 489–496, https://doi.org/10.1016/j.talanta.2006.11.007, 2007.

Ma, L., Guzman, C., Niedek, C., Tran, T., Zhang, Q. and Anastasio, C.: Kinetics and mass yields of aqueous secondary organic aerosol from highly substituted phenols reacting with a triplet excited state, Environ. Sci. Technol., 55(9), 5772–5781, https://doi.org/10.1021/acs.est.1c00575, 2021.

Ma, L., Worland, R., Heinlein, L., Guzman, C., Jiang, W., Niedek, C., Bein, K. J., Zhang, Q. and Anastasio, C.: Seasonal variations in photooxidant formation and light absorption in aqueous extracts of ambient particles, Atmospheric Chemistry and Physics, 24(1), 1–21, https://doi.org/10.5194/acp-24-1-2024, 2024.

McNeill, K. and Canonica, S.: Triplet state dissolved organic matter in aquatic photochemistry: reaction mechanisms, substrate scope, and photophysical properties., Environ. Sci. Process. Impacts, 18(11), 1381–1399, https://doi.org/10.1039/c6em00408c, 2016.

Miller, W. L. and Kester, D. R.: Hydrogen peroxide measurement in seawater by (p-hydroxyphenyl)acetic acid dimerization, Anal. Chem., 60(24), 2711–2715, https://doi.org/10.1021/ac00175a014, 1988.

Smith, J. D., Sio, V., Yu, L., Zhang, Q. and Anastasio, C.: Secondary organic aerosol production from aqueous reactions of atmospheric phenols with an organic triplet excited state., Environ. Sci. Technol., 48(2), 1049–1057, https://doi.org/10.1021/es4045715, 2014.

Wilkinson, F., Helman, W. P. and Ross, A. B.: Rate constants for the decay and reactions of the lowest electronically excited singlet state of molecular oxygen in solution. an expanded and revised compilation, J. Phys. Chem. Ref. Data, 24(2), 663–677, https://doi.org/10.1063/1.555965, 1995.

Zepp, R. G., Wolfe, N. L., Baughman, G. L. and Hollis, R. C.: Singlet oxygen in natural waters, Nature, 267(5610), 421–423, https://doi.org/10.1038/267421a0, 1977.